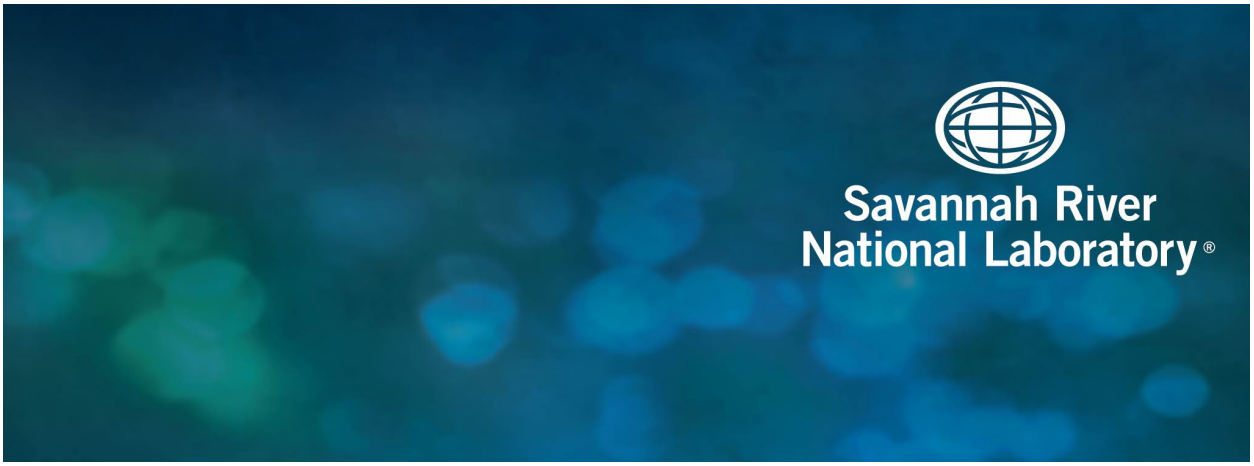

A U.S. DEPARTMENT OF ENERGY NATIONAL LAB • SAVANNAH RIVER SITE • AIKEN, SC • USA

Cation Exchange Capacity, Anion Exchange Capacity, and Mineralogy of F-Area Aquifer Sediments

Holly H. VerMeulen

Hansell Gonzalez-Raymat

September 2023

SRNL-STI-2023-00481, Revision 0

DISCLAIMER

Printed in the United States of America

Prepared for
U.S. Department of Energy

SRNL-STI-2023-00481
Revision 0

Keywords: *CEC, AEC, XRD, aquifer sediments, mineral characterization*

Retention: *Varies*

Cation Exchange Capacity, Anion Exchange Capacity, and Mineralogy of F-Area Aquifer Sediments

Holly H. VerMeulen
Hansell Gonzalez-Raymat

September 2023

Savannah River National Laboratory is operated by Battelle Savannah River Alliance for the U.S. Department of Energy under Contract No. 89303321CEM000080.

REVIEWS AND APPROVALS

AUTHORS:

_____
Holly H. VerMeulen, Environmental Sciences and Dosimetry Date

_____
Hansell Gonzalez-Raymat, Environmental Sciences and Dosimetry Date

TECHNICAL REVIEW:

_____
Miles Denham, Panoramic Environmental Consulting, LLC Date

APPROVAL:

_____
Marion Cofer, Manager Date
Environmental Sciences and Dosimetry

_____
Brady Lee, Director Date
Earth, Biological, and Quantitative System Science

TABLE OF CONTENTS

LIST OF TABLES

LIST OF FIGURES

LIST OF ABBREVIATIONS

AA	Atomic absorption
AEC	Anion exchange capacity
ALTEMIS	Advanced Long-Term Environmental Monitoring Systems
CEC	Cation exchange capacity
EG	Ethylene glycol
IC	Ion chromatography
ICCD	International Centre for Diffraction Data
ICP	Inductively coupled plasma
KCl	Potassium Chloride
LAZ	Lower Aquifer Zone
LBNL	Lawrence Berkeley National Laboratory
MNA	Monitored natural attenuation
PDF	Powder diffraction file
Sr-90	Strontium-90
SRNL	Savannah River National Laboratory
SRS	Savannah River Site
$NaNO_3$	Sodium nitrate
TCCZ	Tan Clay Confining Zone
UAZ	Upper Aquifer Zone
UGA	University of Georgia
wt. %	Weight percent
XRD	X-ray diffraction

1.0 Introduction

Strontium-90 (Sr-90) is a contaminant of concern in groundwater and surface water at both F-Area and H-Area Seepage Basins. This contaminant was disposed of, along with other heavy metals and radionuclides, into a series of unlined seepage basins from 1955 until 1988. The acidity of the wastewater increased Sr-90 mobility from the basin soil through the vadose zone and into the Upper Aquifer Zone (UAZ), creating a groundwater plume that discharges into wetlands areas and a local stream called Fourmile Branch.

In the UAZ, Sr-90 retention is thought to be minimal as the groundwater pH remains highly acidic. However, Denham et al. (2021) evaluated historical monitoring data for wells close to the basins and suggested some Sr-90 sorption could occur in the acidic environment if high cation exchange capacity clays, such as smectite, are present. Besides the UAZ, there is also downward migration of Sr-90 through the Tan Clay Confining Zone (TCCZ) into the Lower Aquifer Zone (LAZ) as the TCCZ is discontinuous across the area and has leaky zones. It is suggested that the vertical migration of Sr-90 into the LAZ started as soon as the acidic pH gradient passed through the TCCZ and into the LAZ. Once in the LAZ, Sr-90 may be attenuated by an increasing pH gradient with increasing depth and higher content of clay minerals, including smectite. Lastly, the wetlands have been sequestering Sr-90 for many years, but the attenuation mechanisms are still unknown.

The current remediation of Sr-90 is through groundwater pH manipulation within the gates of a funnel-and-gate system and beneath the wetland areas as a result of periodic base injections to enhance its attenuation. These base injections will be required until there is no threat of Sr-90 remobilization within the treatment zones. To achieve this, injections must be continued until Sr-90 decays naturally and poses no further threat of remobilization. Therefore, a full understanding of the attenuation mechanisms of Sr-90 is critical to operation of the current remediation and acceptance of monitored natural attenuation (MNA) as the final remedy.

2.0 Purpose

In 2021, a joint effort by Lawrence Berkeley National Laboratory (LBNL), Savannah River National Laboratory (SRNL), and Panoramic Environmental Consulting, LLC was started to investigate the attenuation mechanisms and minerals involved in the sorption of Sr-90 at the F-Area and H-Area Seepage Basins. Denham et al. (2021) began by performing simulations of Sr-90 sorption on single mineral systems identified in the F-Area Seepage Basins. He found kaolinite, goethite, and quartz cannot explain Sr-90 behavior in the base injection treatment zones; so, he hypothesized that the treatment zone monitoring data that showed a protective pH of 5.5 could be explained by the presence of an exchangeable clay, such as illite or smectite, which are known to exist in the aquifer system. To support this hypothesis, SRNL has been conducting characterization studies of F-Area aquifer sediments and lab experiments to firmly establish the protective pH for the gate treatment zones and to parameterize a reactive transport model of Sr-90 behavior at the Savannah River Site (SRS) that will allow better understanding of Sr-90 behavior from basins to wetlands.

The purpose of this document is to summarize the results obtained from the characterization of F-Area aquifer sediments performed at the University of Georgia (UGA). These analyses ultimately help to support strontium adsorption modeling through gaining a better understanding of the adsorption/ion exchange behavior of strontium on aquifer sediments from the SRS's F-Area, which is not well characterized.

3.0 Methods

Through a service subcontract with SRNL, UGA completed several experiments to better inform sorption experiments. Analyses include: 1) clay mineral analysis to identify the presence and relative amounts of different minerals in these soils; including smectite, illite, goethite, and kaolinite, 2) measurements of the cation exchange capacity (CEC) of the bulk soil samples, and 3) anion exchange measurements for the sediments. The results of these analyses are summarized in this report.

3.1.1.1 Sample collection

For the characterization study, F-Area aquifer sediments were collected from soil cores stored in the SRS Core Facility at discrete depths representing the UAZ, LAZ, and TCCZ (Figure 3-2). Two core samples (FSB-78A and FAW-05) were selected from locations downgradient of the seepage basins along the plume centerline that has been exposed to the acidic groundwater plume for decades. The other core sample (FSB-76A) has not been exposed to the groundwater plume and is used for comparison (Figure 3-1). Each of the cores was sampled at discrete depths, and subsamples of the bulk sediments were provided to UGA for clay mineral analysis, as well as CEC and anion exchange capacity (AEC) measurements.

Samples collected include:

- FSB-78
    - TCCZ: at 108 ft and 118 ft (about 10 ft below the other TCCZ sample)
    - LAZ: just below the Tan Clay at 124 ft and about 10 ft below the other LAZ sample at 134 ft
- FSB-76
    - TCCZ: at 108 ft
    - LAZ: just below the Tan Clay at 114 ft and about 10 ft below the other LAZ sample at 124 ft
- FAW-05
    - Upper UAZ: at 49 ft
    - Mid UAZ: at 59 ft
    - Lower UAZ: at 68 ft

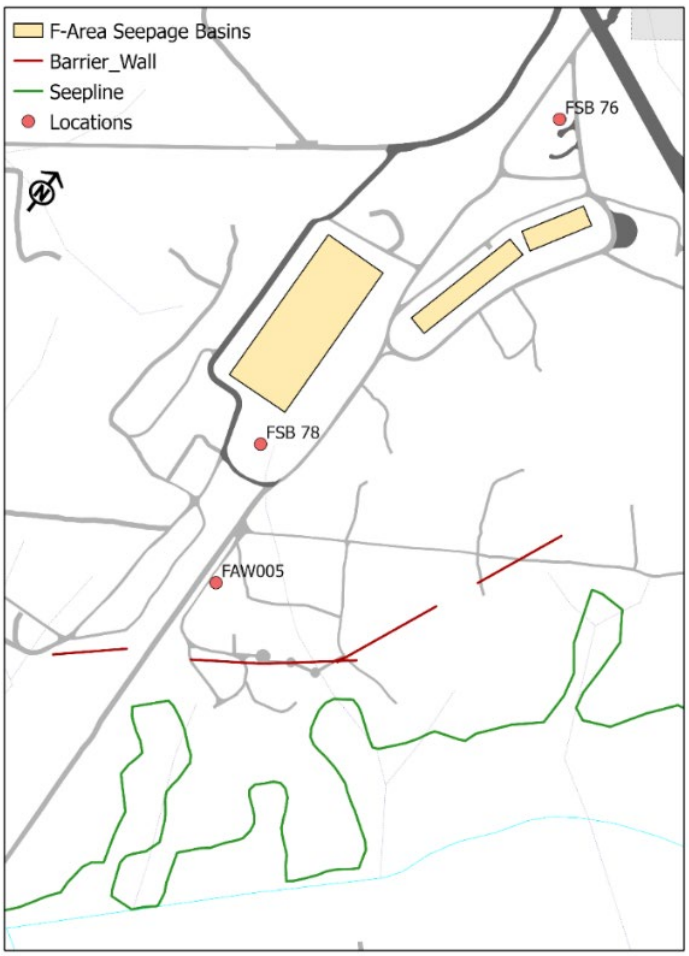

Figure 3-1. Soil core sampling locations

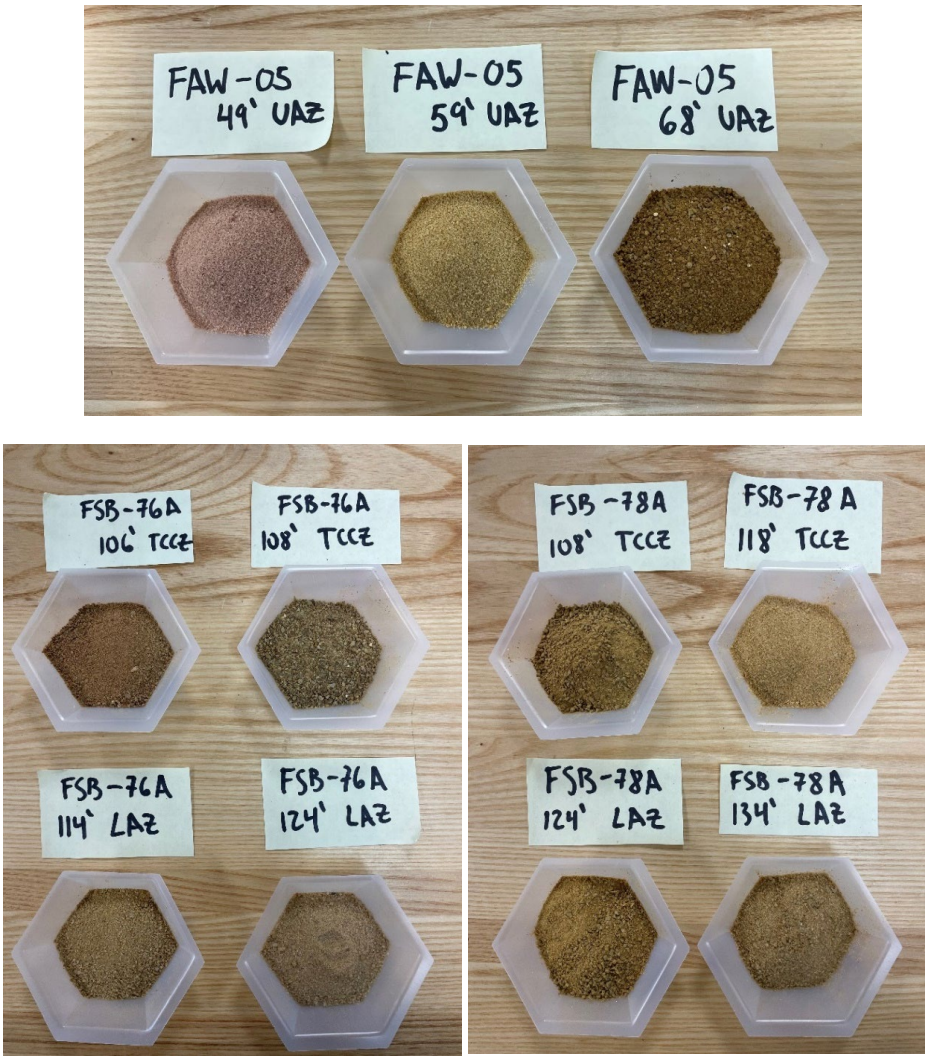

Figure 3-2. F-Area aquifer sediment collected from UAZ, TCCZ, and LAZ

3.2 Cation Exchange Capacity (CEC) and Anion Exchange Capacity (AEC)

CEC refers to the capacity of a mass of soil material to retain cations on charged surfaces in the colloid fraction of the soil. It describes the number of negatively charged sites on a soil material. This is typically determined by displacing adsorbed cations like calcium, magnesium, sodium, potassium, and aluminum with a neutral salt, such as barium dichloride, and measuring the displaced cations using atomic absorption (AA) or inductively coupled plasma (ICP) spectroscopy. Alternatively, a cation such as ammonium may be used to fully saturate the exchange sites of a sample, then displaced and measured as an estimate of CEC. AEC, or the number of positive sites, can also be measured in this method by determining retention of an associated anion such as nitrate or chloride. Anion concentrations are determined by IC or colorimetry. CEC and AEC are important surface chemical properties related to nutrient status and contaminant behavior in soil/sediment systems. In our study, UGA followed a batch procedure that is described in detail the sections below.

3.2.1 Reagents

- 0.01 M Potassium Chloride
- 0.5 M Sodium Nitrate

3.2.2 Procedure

3.2.2.1 Exchanging (entrained solution)

- Label and weigh each empty 50-mL centrifuge tube to 0.001 g
- Place 5 g of air-dried, milled soil into each 50-mL prelabeled and pre-weighed centrifuge tube
- Add 40 ml of 1 M Potassium Chloride (KCl) and shake (124.5 rpm) overnight (at least 15 hours) using a reciprocal shaker
- Centrifuge and discard the supernatant
- Wash five times with 30-40 mL of 0.01 M KCl and discard.
    - At the final washing, centrifuge and decant the final supernatant, but retain for K^+ and Cl^- determination (C1)
    - Note: The supernatant from each centrifugation should be clear. Don't lose any soil particles during this decanting.
- Weigh the tubes to obtain the volume (V1) of entrained solution in the sediment in order to determine entrained K^+ and Cl^-. It is assumed that the concentrations of the entrained K^+ and Cl^- are equal to those of the final washing solution.

3.2.2.2 Displacement

- Wash 4 times with 25 ml of 0.5 M Sodium Nitrate ($NaNO_3$) to displace the adsorbed K^+ and Cl^-.
- Centrifuge and decant the exchanging solution into a 100-mL volumetric flask (V2) that is brought to volume and subsequently analyzed for K^+ and Cl^- (C2)
- Calculate the CEC (K^+; Equation 1) and the AEC (Cl^-; Equation 2) as centimoles of charge per kilogram
- Weigh a separate amount of each soil and dry at 105 degrees Celsius to get the ratio of dry soil weight/wet soil weight

$$CEC\ \left(\frac{cmol}{kg}\right) = \frac{0.1\ (C2V2 - C1V1)}{39\ W}$$ .....Equation 1

where:

C1 = concentrations (mg/L) of K+ and Cl- in final washing solution of 0.01 M KCl
C2 = concentrations (mg/L) of K+ and Cl- in the displacing solution of 0.5 M NaNO3
V1 = volume (ml) of the solution entrained in sediments after the final washing of 0.01 M KCl
V2 = total volume (ml) of the displacing of 0.5 M NaNO3,
39 = atomic weight of K+
W = weight (g) of oven-dried soil sample at 105 degrees Celsius

$$AEC\ \left(\frac{cmol}{kg}\right) = \frac{0.1\ (C2V2 - C1V1)}{35.5\ W}$$ .....Equation 2

where:

C1 = concentrations (mg/L) of K+ and Cl- in final washing solution of 0.01 M KCl,
C2 = concentrations (mg/L) of K+ and Cl- in the displacing solution of 0.5 M NaNO3
V1 = volume (ml) of the solution entrained in sediments after the final washing of 0.01 M KCl
V2 = total volume (ml) of the displacing of 0.5 M NaNO3
35.5 = atomic weight of Cl-, and
W = weight (g) of oven-dried soil sample at 105 degrees Celsius

3.3 X-Ray Diffraction (XRD)

The sediment samples (bulk and clay fraction (< 2 μm)) were characterized using X-Ray Diffraction (XRD), which is a nondestructive technique that allows identification of minerals in the sample based on the

crystallographic structures present. Additional information can be obtained if very detailed XRD is done. For the mineral characterization, a Bruker D8 Advance X-ray Diffractometer instrument was used for the analysis. The XRD instrument was set up with a 250 cm goniometer radius, a 0.6 mm divergent slit, and Bragg-Bentano geometry.

Approximately 15 grams of each wet sample were taken for bulk mineralogy and dried in an oven at 65°C overnight. A corundum mortar was then used to manually grind about 7 g of the dried sample. To further reduce the powder's particle size to an average of 5 to 10 µm, 10 ml of ethyl alcohol (EG) was added to the powder and processed in a McCrone micronizing mill for 10 minutes. Samples were backfilled against a square plate glass into a 2.5 x 2.5 cm aluminum holder after being dried to eliminate alcohol in a 65°C oven overnight. To create a flat, self-supporting mount, the powder was compressed at 400 psi. The goal was to retain the sample geometry tangential to the instrument-focusing circle and reduce sample transparency before it is placed within the instrument.

To reduce low-angle dispersion into the position-sensitive Lynx-Eye® detector, a knife edge blade was put 2 mm over the sample's surface. To reduce Kb radiation, an iron filter was utilized in conjunction with a cobalt radiation source (Kα1 = 1.7890Å and Kα2 = 1.7928Å) that was operated at 35 kV and 40 mA. To verify alignment and calibration within 0.01° 2-theta tolerance of the certificate value for the brightest reflection peak position, an external NIST Reference standard SRM1976b corundum (α-Al2O3) was used. Using a locked-coupled continuous scan mode with a step size of 0.01° 2Θ and a count rate of 0.2 seconds per step, the scan range was enhanced from 2 to 70° 2Θ. The Bruker Eva® program presents raw data and graphs known as diffractograms with patterns and peak positions identified. The raw data was then Kα2 stripped. Peak locations were compared to information from the powder diffraction file (PDF) database of the International Centre for Diffraction Data (ICDD).

Eva software was used with the 2022-PDF database to identify the best-fit phases for mineral identification. A structure file containing the unit cell lattice parameters, atom types, and atomic positions was exported for each phase found. Semi-quantitative models of samples were analyzed using TOPAS® software. The Rietveld refining method is the basis of this program. Using kinematic diffraction theory, this method determines the theoretical diffraction pattern for each phase. The disparity between observed XRD data and predicted patterns is then reduced using optimization techniques. The TOPAS software has choices for optimizing structure file data and other factors, including preferred orientation, crystal planes, and mean coherent scattering domain size. Additionally, the procedure enhances total XRD intensity, which is associated with abundance and explains the weighted profile R-factor (Rwp), which was used to assess the goodness-of-fit of each modification. For semi-quantitative analysis, model solutions with Rwp 15 are typically acceptable. It is significant to highlight that mixed-layer structures cannot be considered in the TOPAS® software calculations. As a result, despite additional optimization attempts in some circumstances, adequate Rwp values were not obtained. Despite this restriction, consistent procedures were employed to maintain model parameters with comparable ranges of values to enable inter-sample comparison of relative abundances.

For the fine clay fraction, 10 g of dried sample were added to a centrifuge tube containing 38 g of sodium hexametaphosphate and 8 g of sodium carbonate in 1 L of deionized water. The mixture was stirred for about 1 minute using a Branson Sonifier Cell Disrupter 350. After that, samples were sieved to remove particles > 63 µm (230 mesh) to eliminate the sand fraction. Using conventional centrifugation methods, the silt fraction, which is 63 µm in size, was separated from the 2-micron clay fraction. Following this procedure, the resulting slurry was deemed to be Na-saturated. For Mg-saturated samples, this process was repeated, and samples were prepared by exchanging in 0.1 M $MgCl_2$ solutions. The slurry was centrifuged to settle all the particles with adequate velocity and duration. Solution renewal and centrifugation processes were repeated until full saturation was achieved. The slurry was given deionized water, and additional centrifugation was used to eliminate extra salt. This fine fraction was mixed with 25 to 30 mL of deionized

water, pipetted onto a glass petrographic slide (25 mm × 40 mm), and airdried overnight. The sample was kept in EG overnight in a closed EG atmosphere and heated in the oven for an hour at 110°C, 350°C, and 550°C. During the drying process, orientated particles are produced, which improve the phyllosilicate/clay minerals' basal reflections.

Semi-quantitative analysis was performed using the Mg-saturated EG samples and the TOPAS® Rietveld software. Bias was given to the basal reflections of the phyllosilicates, to accommodate their oriented state of sample mounting.

4.0 Results

4.1 XRD

Clay mineral analysis results allow for the determination of minerals dominating strontium sorption and will inform contaminant behavior for use in fate and transport modeling efforts. Determining the minerals that dominate strontium sorption in F-Area aquifer sediments is an important component for characterizing strontium behavior and designing effective treatment strategies for this contaminant. Minerals of particular interest in the aquifer sediments include smectite, illite, goethite, quartz, and kaolinite. The mineralogy of the aquifer sediments will impact contaminant behavior, reactivity, and transport in these systems. Mineralogy analysis is accomplished through specialized sample preparation and XRD analysis. Resulting diffraction patterns are unique to each clay mineral type and can be used to distinguish between them and quantify each fraction.

XRD bulk and XRD clay analyses are summarized in Table 4-1 (Figure 4-3) and Table 4-2, respectively. Raw XRD spectra are also included in the Attachments section of this report (Figure 6-1 through Figure 6-39).

Bulk XRD analyses indicate, on average, that quartz is the dominant mineral, ranging from 36 to 94 wt. %. Quartz is the most prevalent mineral, particularly in the UAZ and LAZ samples, as expected. Quartz composed the largest fraction of the following sediments: FAW-05 (UAZ 49 ft), FAW-05 (UAZ 59 ft), FSB-76A (LAZ 114 ft), FSB-76A (LAZ 124 ft), FSB-78A (LAZ 134 ft), and FSB-78A (TCCZ, 118 ft). This is in good agreement with previous characterization of SRS F-Area sediments that confirmed that they are primarily composed of quartz sand (Dong et al., 2012).

For all other sediments, kaolinite is the primary mineral, including FAW-05 (UAZ, 68 ft), FSB-76A (TCCZ, 108 ft), FSB-78A (LAZ, 124 ft), and FSB-78A (TCCZ, 108 ft). Kaolinite, a secondary mineral, is the second most abundant mineral overall, ranging from 2 to 52 wt.%. ‘Secondary’ in this text designates minerals that were formed by the alteration of original minerals that were deposited in the formation. For example, microcline (feldspar) dissolves incongruently leaving kaolinite. This high kaolinite content also mirrors previous analysis of F-Area sediments where goethite and kaolinite were identified as the major mineral components of the fine fractions (Dong et al., 2012). Goethite ranges from 1 to 14 wt.%, while illite (or degraded micas) ranges in abundance from 2 to 19 wt.%. Illite is an exchanging clay that has been shown to play a role in contaminant migration of radionuclides like Sr^{90}, by promoting cation sorption (Missana et al., 2008). Bulk XRD analysis does not distinguish vermiculite from smectite, hence quantitation was grouped as expandable 2:1 clays. Content of 2:1 expandable clay ranged from 0 to 6 wt.%. Microcline ranged from 0 to 4 wt.%.

A minor phase occurred in three samples, which produced a weak peak in the diffractogram (Appendix A). Assignment of that peak was tentatively made to garnet; however, the certainty of that assignment is weak. Nevertheless, the presence of garnet in the samples is reasonable because the original source rocks for all of the samples include metamorphic rocks that contain garnet.

Bulk XRD results also give information about the change in mineral composition with depth. The vertical profiles of these values (Figure 4-1) show that quartz dominates the mineral composition (> 85%) in the upper and middle part of the UAZ. But as the lower part of the UAZ is approached and then the TCCZ is reached, quartz composition is reduced to ~30% (except FSB78A 118 ft which has 69%). In the LAZ, quartz increases again to ~60% of the total bulk fraction. The opposite trend to quartz is seen in kaolinite concentrations. In the upper and middle portion of the UAZ, kaolinite represents only ~ 6%. The kaolinite fraction is highest in the lower part of the UAZ and TCCZ, then decreases in the LAZ (except for FSB-78A 124 ft). As the bottom of the UAZ and TCCZ are approached, kaolinite presence is increased to 40-50%, but then decreases to between 3-38% in the LAZ. Goethite content (1-3%) in the bulk sediment is fairly similar in the UAZ, TCCZ, and LAZ, with its content only increasing (14%) in the bottom part of the UAZ. Other mineral contents in the bulk sediments generally do not change much between the different aquifer zones.

Table 4-1. Bulk XRD Analyses of F-area Aquifer Sediments.

	Bulk XRD weight percent (error ± 10% of values listed)						
Sample ID	**Quartz**	**Garnet**	**Microline**	**Kaolinite**	**Illite**	**Smectite**	**Goethite**
FAW-05-UAZ_49	94	1	0	2	2	0	2
FAW-05-UAZ_59	86	1	0	6	4	0	3
FAW-05-UAZ_68	29	0	0	40	17	0	14
FSB-76A-TCCZ_108	28	0	3	52	12	3	2
FSB-76A-LAZ_114	66	0	0	25	8	1	2
FSB-76A-LAZ_124	88	1	0	3	8	0	1
FSB-78A-TCCZ_108	36	0	2	41	13	5	3
FSB-78A-TCCZ_118	69	0	4	17	6	3	2
FSB-78A-LAZ_124	36	0	3	38	14	6	2
FSB-78A-LAZ_134	60	0	2	26	8	4	1

Note: Red columns considered primary minerals, while green columns considered secondary minerals.

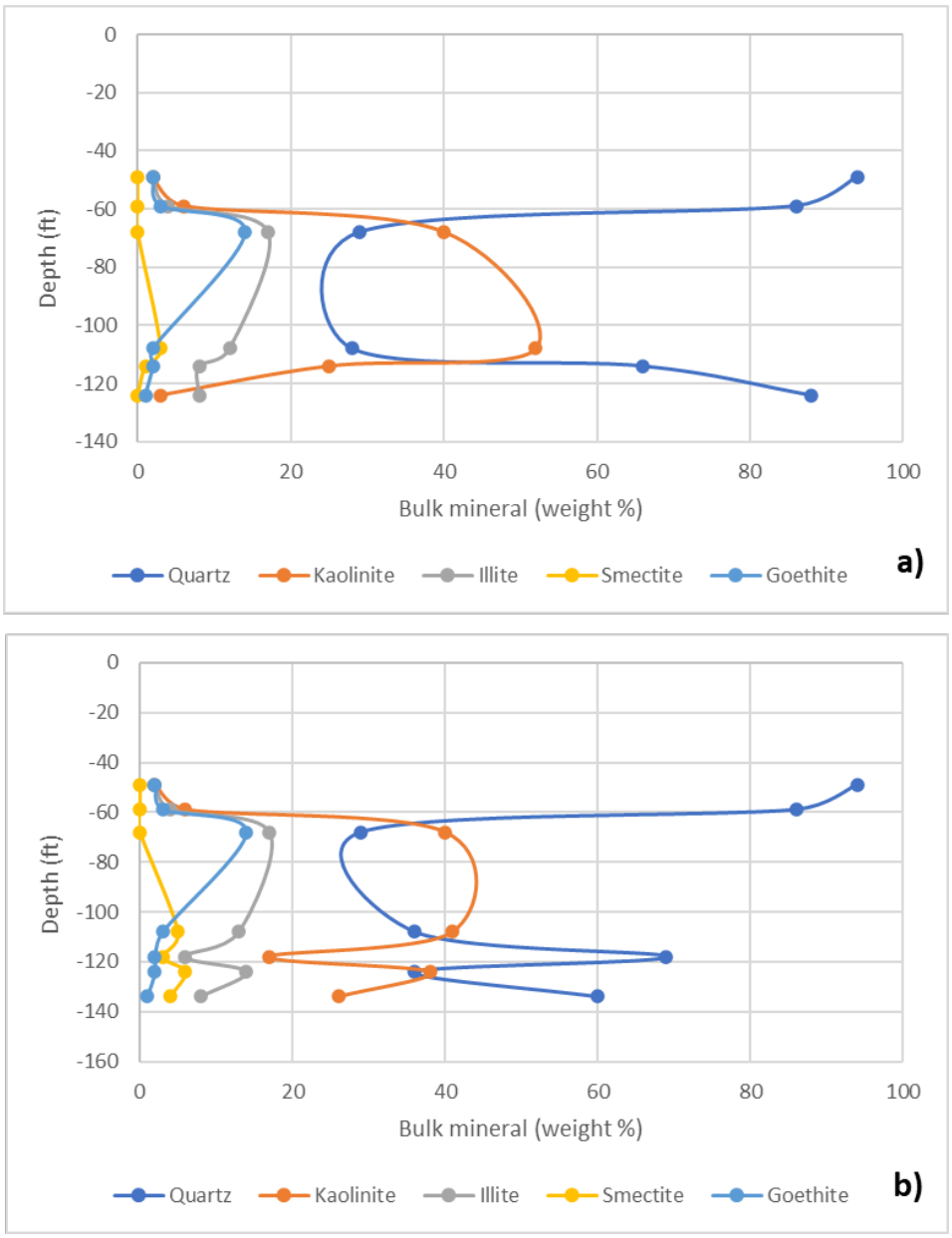

Figure 4-1. Mineral composition depth profile for bulk sediment samples a) FAW-05 and FSB-76 and b) FAW-05 and FAB-78

The clay fraction analysis of the samples in Mg-saturated states (air-dried, EG, 110°C, 350°C, and 550°C) allowed for more detail identification of fine phases (Table 4-2). Kaolinite is confirmed by collapse of its structure at ~7.1Å upon heating to 550°C. Goethite is confirmed by collapse of its structure at 4.14Å at 350°C. The occurrence of peaks at ~17Å shifting to larger d-spacings from air-dried to EG (under EG solvation) and collapse to 10Å upon hearing indicated the presences of expandable 2:1 structures. All samples were Mg-saturated, which is an ion that has a high valance and hydration energy. Samples that expanded to 17Å are listed as smectite clays.

Fine fraction XRD analyses display different trends than those seen in bulk analysis results (Figure 4-2). In the fine fractions (< 2 µm), kaolinite and smectite tend to dominate the mineral composition of most samples

(Table 4-2). Kaolinite is highest in the UAZ sediments, ranging between 67 and 91 weight percent. But in the TCCZ and LAZ sediments, kaolinite decreases and smectite becomes the most abundant mineral (36-89%). Goethite content is highest at the bottom of the UAZ, as seen in the bulk sediment analysis results. Illite content is high in the upper part of the UAZ (26 wt. %), drops down to $\leq$ 2 wt. % in the middle/lower UAZ and LAZ. In the FSB-78 sample, illite content increases to a maximum in the TCCZ (47 wt. % at 118 ft), but this trend is not seen in FSB-76 results. Quartz content is minimal in the fines fractions for all sediments throughout all zones, as expected; 3-7 wt. % in FSB-78, 2-4 wt. % in FAW-05, and 1-2 wt. % in FSB-76.

Table 4-2. XRD Analyses of F-area Aquifer Sediment Fine Fractions.

	Fine fraction (< 2 µm) weight percent					
Sample ID	**Quartz**	**Kaolinite**	**Smectite**	**Illite**	**Goethite**	**CarFap**
FAW-05-UAZ_49	3	67	0	26	4	0
FAW-05-UAZ_59	2	91	0	2	5	0
FAW-05-UAZ_68	4	81	0	2	14	0
FSB-76A-TCCZ_108	1	1	97	0	0	0
FSB-76A-LAZ_114	2	3	94	1	1	0
FSB-76A-LAZ_124	2	5	90	2	1	0
FSB-78A-TCCZ_108	6	14	54	25	0	1
FSB-78A-TCCZ_118	7	10	36	47	0	0
FSB-78A-LAZ_124	7	1	91	1	0	0
FSB-78A-LAZ_134	3	0	89	1	0	7

CarFap = carbonate fluorapatite. Illite includes degraded mica.

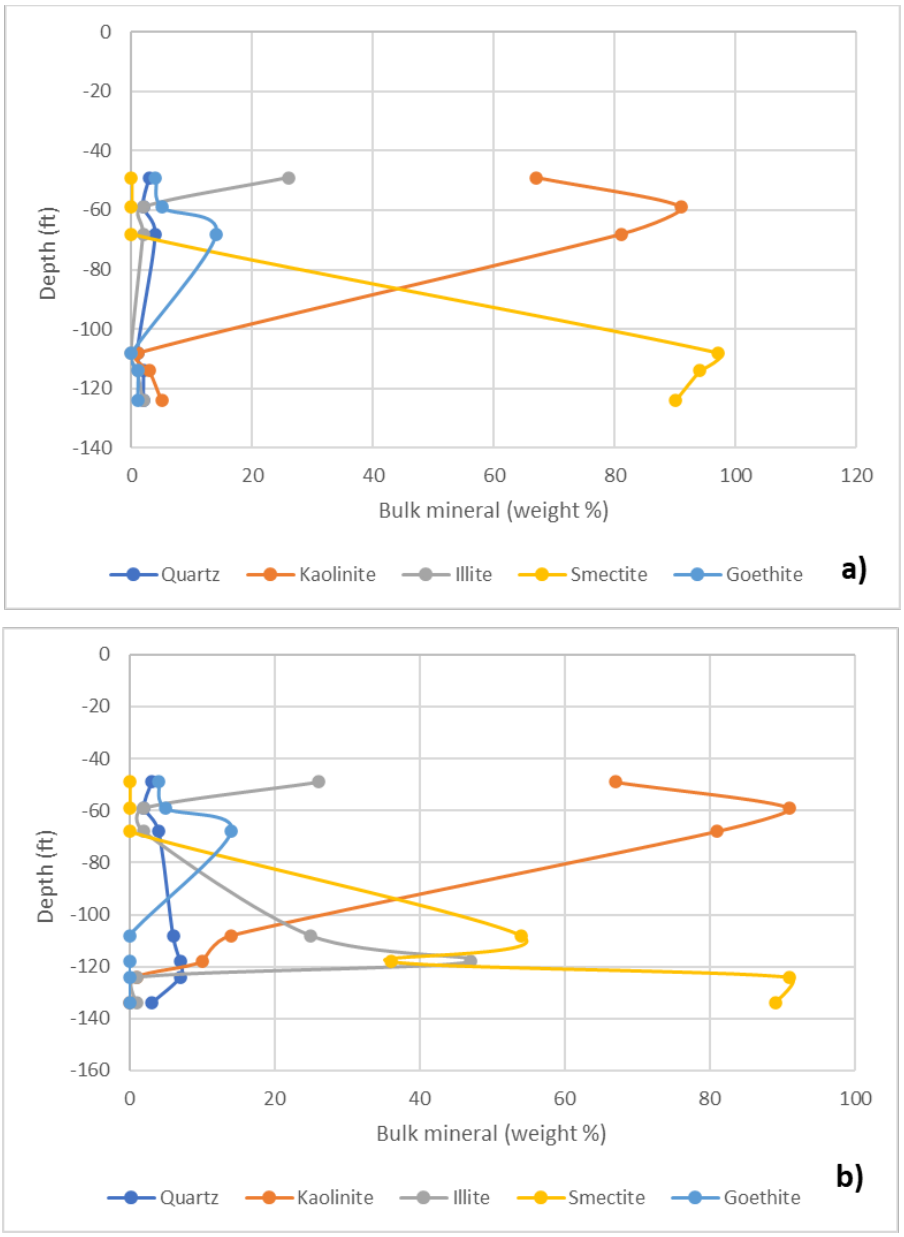

Figure 4-2. Mineral composition depth profile for fine fractions of sediment samples a) FAW-05 and FSB-76 and b) FAW-05 and FAB-78

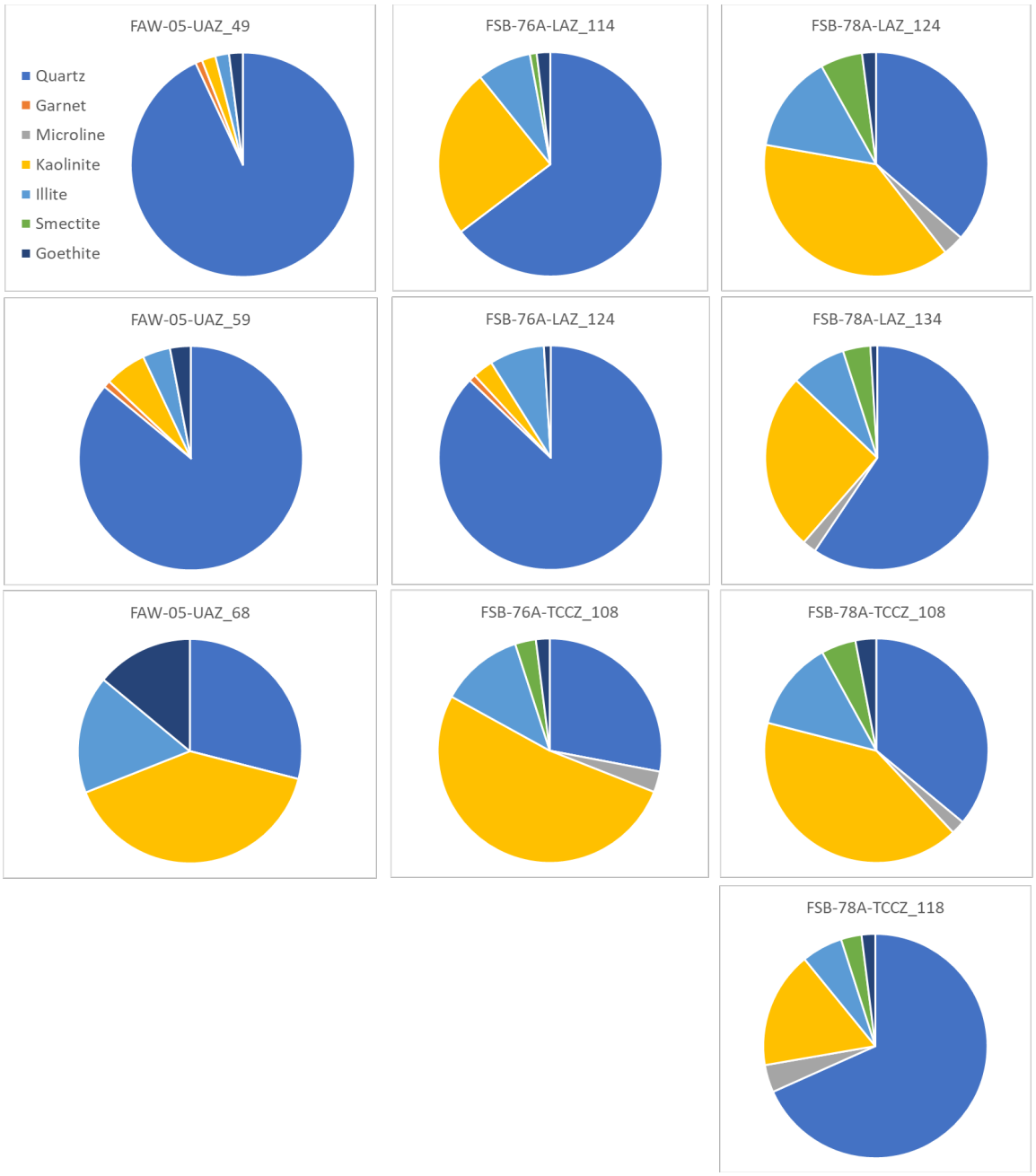

Figure 4-3. XRD Analyses of Bulk F-area Aquifer Sediments

4.2 CEC and AEC

Table 4-3 compares measured CEC and AEC values for each sediment. As expected, quantified CEC values are higher than AEC values for all aquifer sediments. CEC values ranged from 0.09 cmol/kg to 21.02 cmol/kg, while AEC values ranged from below detection (< 0.03 cmol/kg) to 0.35 cmol/kg.

FSB-78A samples had higher overall CEC values than FAW-05 and FSB-76A sediments. Samples collected from the TCCZ also typically had higher CECs than those from the LAZ for both FSB-78A and FSB-76A (with the exception of FSB-78A collected at 118 ft). This can possibly be attributed to the mineral composition of the sediments. FSB-78A sediments have higher clay contents than the other soils on average,

which would increase the CEC values. A higher clay content, particularly when composed of smectite and other mixed clays, results in higher CEC values because clays have a higher surface area than quartz grains and smectite has a higher CEC compared to other clay; thus, making them more likely to contribute to the sorption of cations like strontium.

FSB-76A samples have not been exposed to contamination (or were exposed to very little), while the other two samples have been exposed for decades. However, the CEC of FSB-76A and FAW-05 are comparable, supporting that the acidic groundwater plume likely did not impact that sorptive property.

Table 4-3. CEC and AEC Analyses of F-area Aquifer Sediments.

Sample ID	CEC (cmol/kg)	AEC (cmol/kg)
FAW-05-UAZ_49	7.7	0.09
FAW-05-UAZ_59	0.09	0.06
FAW-05-UAZ_68	5.04	0.35
FSB-76A-TCCZ_108	6.87	0.07
FSB-76A-LAZ_114	3.01	0.03
FSB-76A-LAZ_124	1.26	0.03
FSB-78A-TCCZ_108	21.02	0.26
FSB-78A-TCCZ_118	4.22	0.03
FSB-78A-LAZ_124	12.34	0.03
FSB-78A-LAZ_134	8.59	0.03

The vertical profile for the CEC values for the FAW05/FSB76A system is very similar to kaolinite and illite patterns for the bulk mineral composition (Figure 4-4). This could indicate that these two minerals dominate the cation exchange of those sediments. In the case of FAW005/FSB78A, it is likely that illite and smectite dominate the cation exchange capacity since the CEC vertical profile is similar to the fine fraction.

AEC did not exhibit any trends and was low in all samples, especially compared to reported CEC values. FAW-05 had a higher AEC than the other two sediments, with the highest capacity for FAW-05 at 68 ft. AEC values may also be correlated with mineralogy. For instance, the sample with highest AEC is also that with the highest goethite concentration. A possible correlation (R^2 = 0.701) between AEC and goethite weight percent was found (Figure 4-5). This comparison plot assumes AEC values below the detection limit were assigned a value of half the minimum (i.e., 0.01 cmol/kg). The positive correlation is consistent with the notion that goethite has AEC at circum-neutral pH condition.

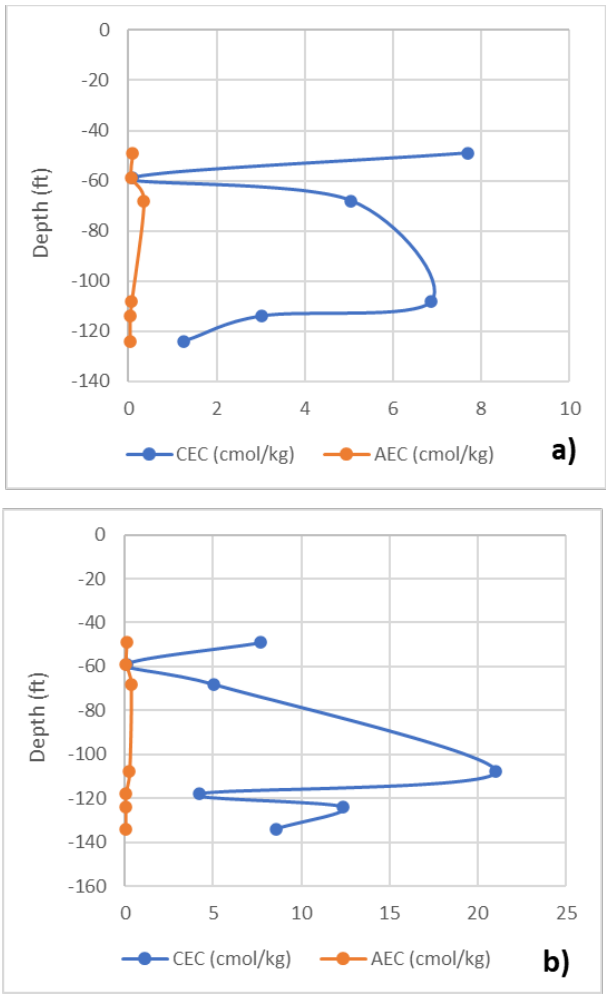

Figure 4-4. Cation exchange capacity and anion exchange capacity values for a) FAW-05 and FSB-76 and b) FAW-05 and FAB-78

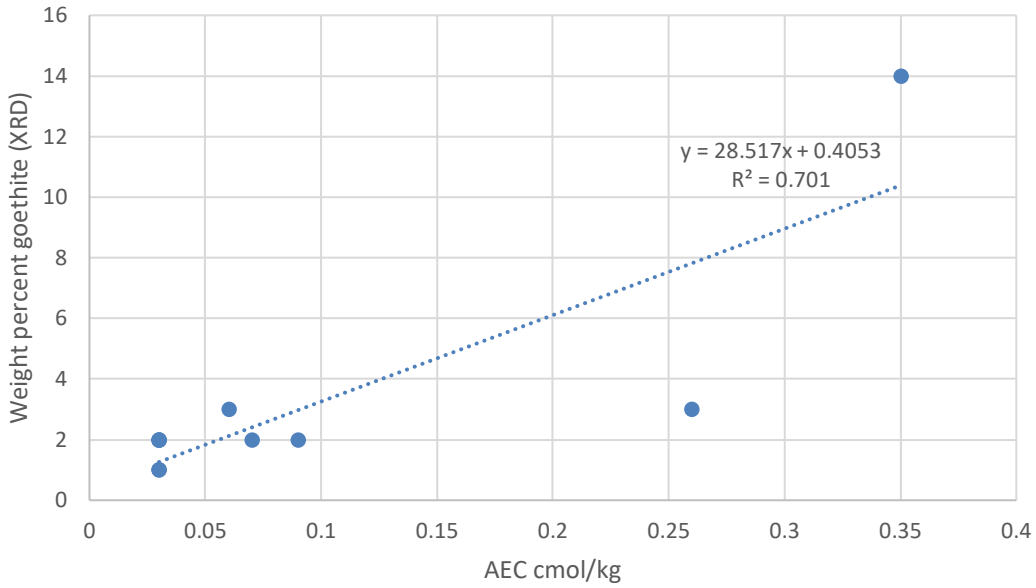

Figure 4-5. AEC versus bulk fraction goethite (weight %).

Using the assumptions in Table 4-4, Figure 4-6 is a plot of measured CEC values versus the combined illite and smectite content (wt. %) in the bulk samples. A generally positive correlation exists between the two independent measures. This supports the notion that the clay minerals are responsible for CEC response measured, with a further idea that a nominal amount of expanding clay can have a large impact on the CEC properties of a sample.

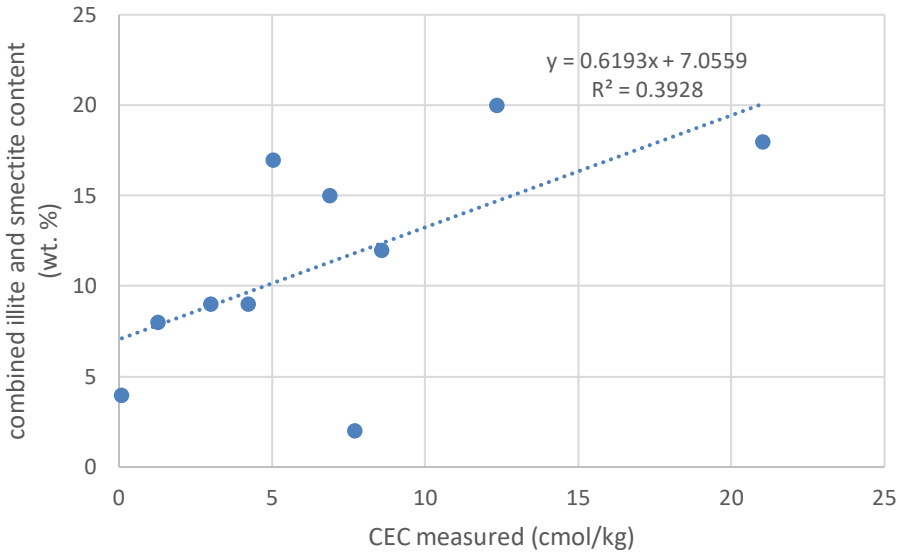

Figure 4-6. Measured CEC versus clay (illite and smectite) content from bulk XRD mineralogy

Table 4-4. Sum of primary (red) and clay minerals (green).

Sample ID	Sum % primary minerals	Sum % clay minerals	Weighted CEC < 2 µm	Weighted CEC kg clay/kg sample
FAW-05-UAZ_49	94.3	3.9	13.4	0.5
FAW-05-UAZ_59	86.8	10.5	9.8	1.0
FAW-05-UAZ_68	28.7	57.4	9.0	5.2
FSB-76A-LAZ_114	65.8	33.6	47.5	15.9
FSB-76A-LAZ_124	89.2	10.2	46.2	4.7
FSB-76A-TCCZ_108	31.2	66.9	48.7	32.6
FSB-78A-LAZ_124	39.8	58.2	46.1	26.8
FSB-78A-LAZ_134	61.6	37.5	44.9	16.8
FSB-78A-TCCZ_108	38.5	58.1	34.4	20.0
FSB-78A-TCCZ_118	73	25.5	30.8	7.8

	Quartz	Kaolinite	Smectite (2:1)	Illite	Goethite	CarFap
Assumed CEC (cmol/kg)	1	10	50	25	3	1

Note: Weighted sums of CEC were calculated using assumed CEC values for individual mineral (gray row) and mineral abundances in the < 2 µm fine fraction. Weighted CEC values for each sample were normalized by the relative abundance of clay minerals in the bulk samples.

5.0 Conclusions

- Quartz, microline, and garnet were identified as primary minerals, while kaolinite, illite, smectite, and goethite were identified as secondary clay minerals, by XRD analysis.
- Quartz was found to be the most abundant mineral in the majority of aquifer sediment samples, ranging from 36 to 94 wt. %. For all other sediments, kaolinite is the primary mineral (2 to 52 wt.%).
- CEC values ranged from 0.09 cmol/kg to 21.02 cmol/kg, while AEC values ranged from below detection (< 0.03 cmol/kg) to 0.35 cmol/kg
- CEC/AEC values may be correlated with the mineral composition of the sediments. This is supported by a somewhat high (R^2= 0.7) correlation between goethite content and CEC, as well as a generally positive correlation between measured CEC values and the weighted XRD CEC values determined.

6.0 References

Denham et al (2021) Conceptual Model of Sr-90 Behavior in Groundwater of the F- and H-Area Seepage Basins, Savannah River Site: Potential Attenuation Mechanism, Panoramic Environmental Consulting, LLC, PanEnv-2021-002.

Dong et al. (2012) Uranium (VI) Adsorption and Surface Complexation Modeling onto Background Sediments from the F-Area Savannah River Site, Environmental Science & Technology, 46, 1565-1571.

Missana et al. (2008) Sorption of Strontium onto Illite/Smectite Mixed Clays, Physics and Chemistry of the Earth, Parts A/B/C, 33 (1) 156-162.

Appendix A. XRD Spectra

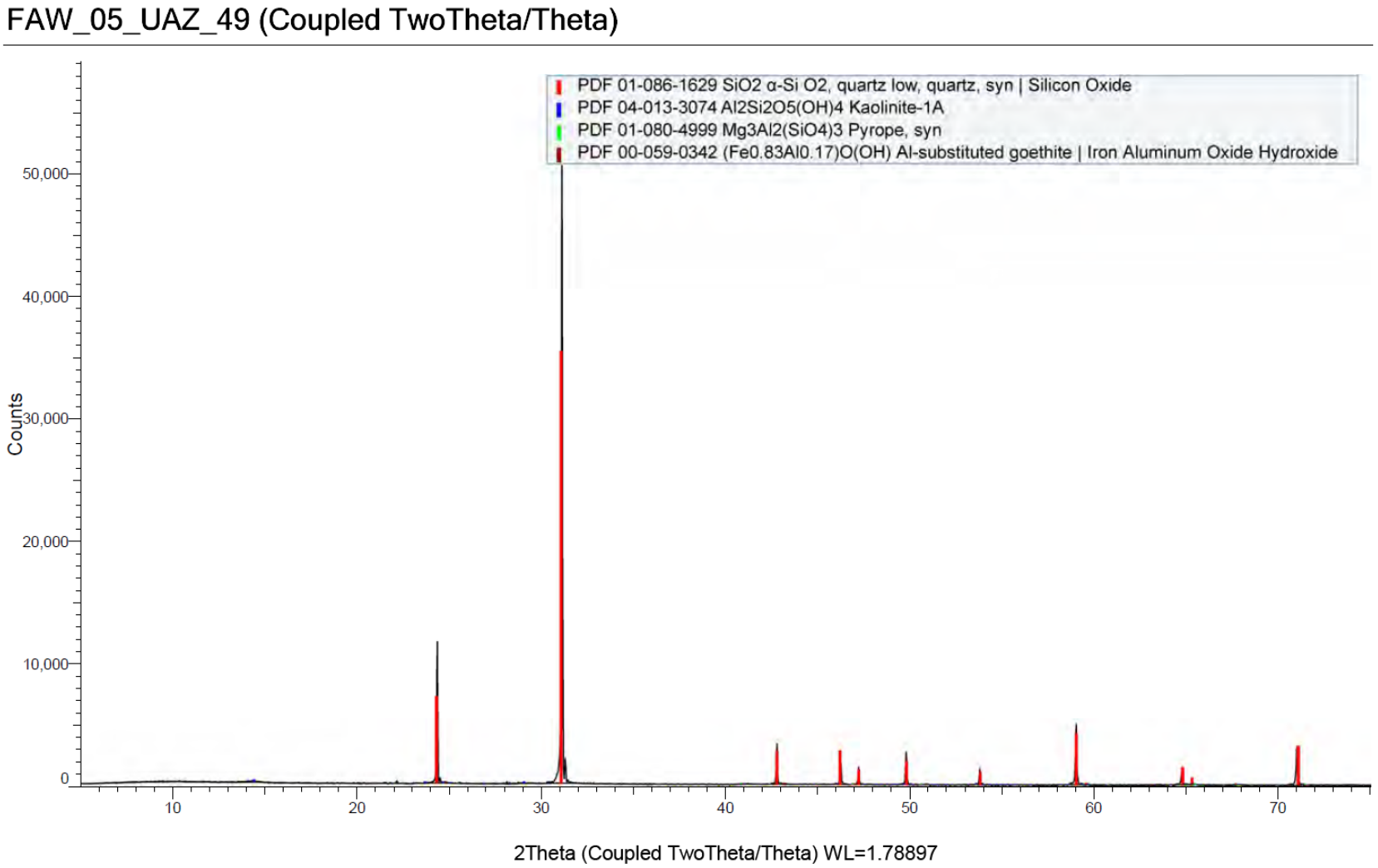

Figure 6-1. Bulk XRD diffraction pattern: FAW-05, UAZ, 49 ft

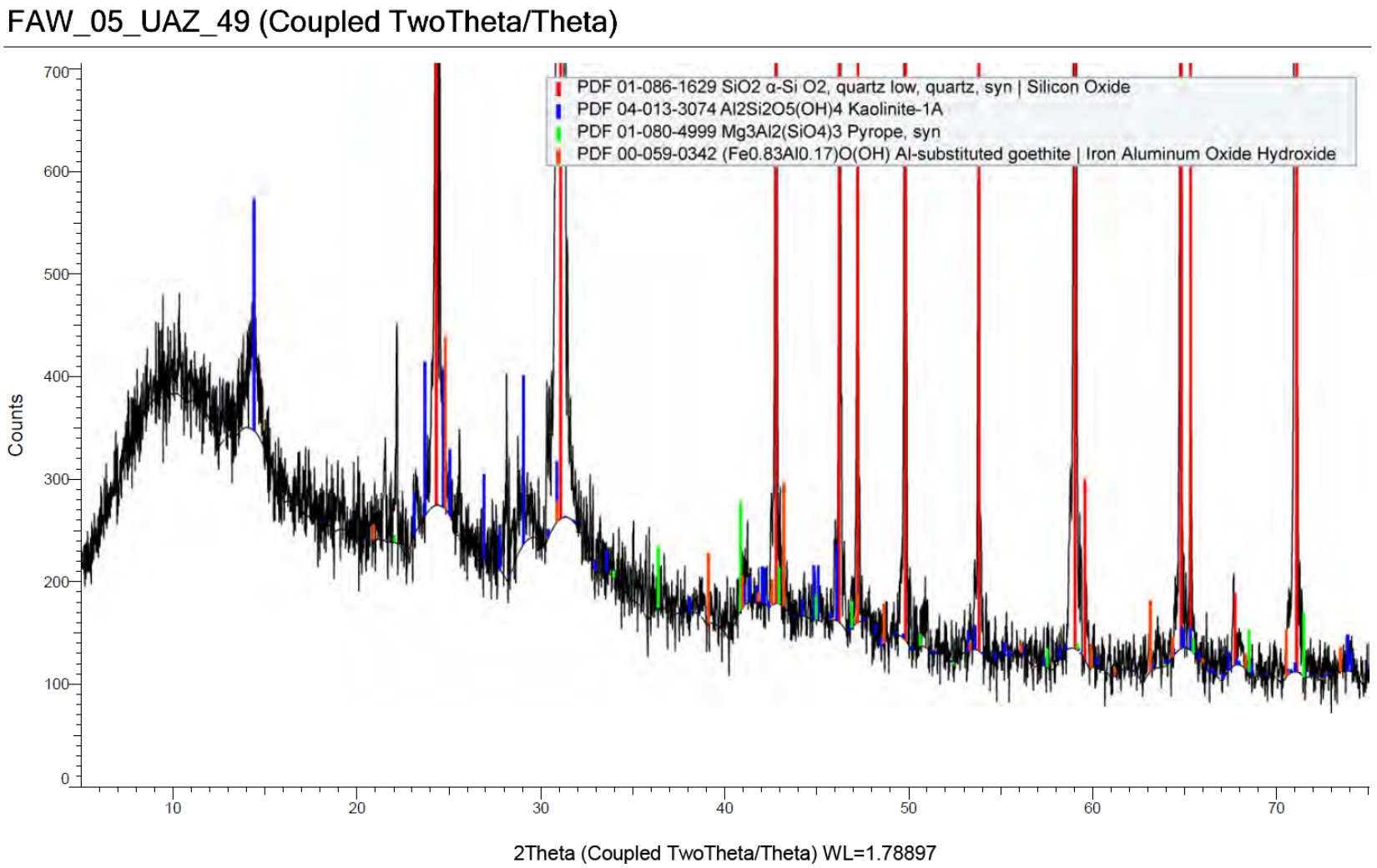

Figure 6-2. Zoomed bulk XRD diffraction pattern: FAW-05, UAZ, 49 ft

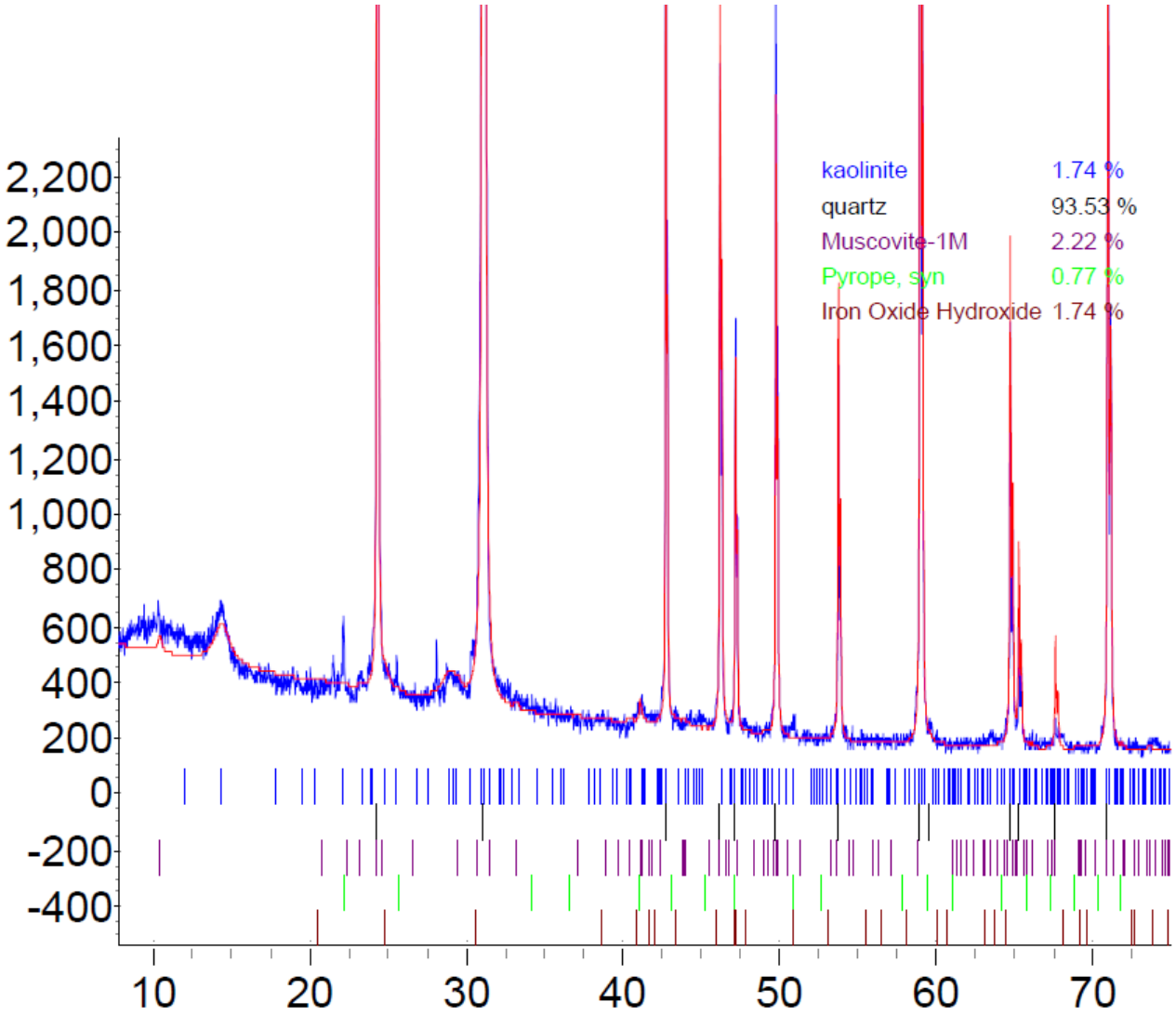

Figure 6-3. Bulk XRD identification and semi-quantification: FAW-05, UAZ, 49 ft

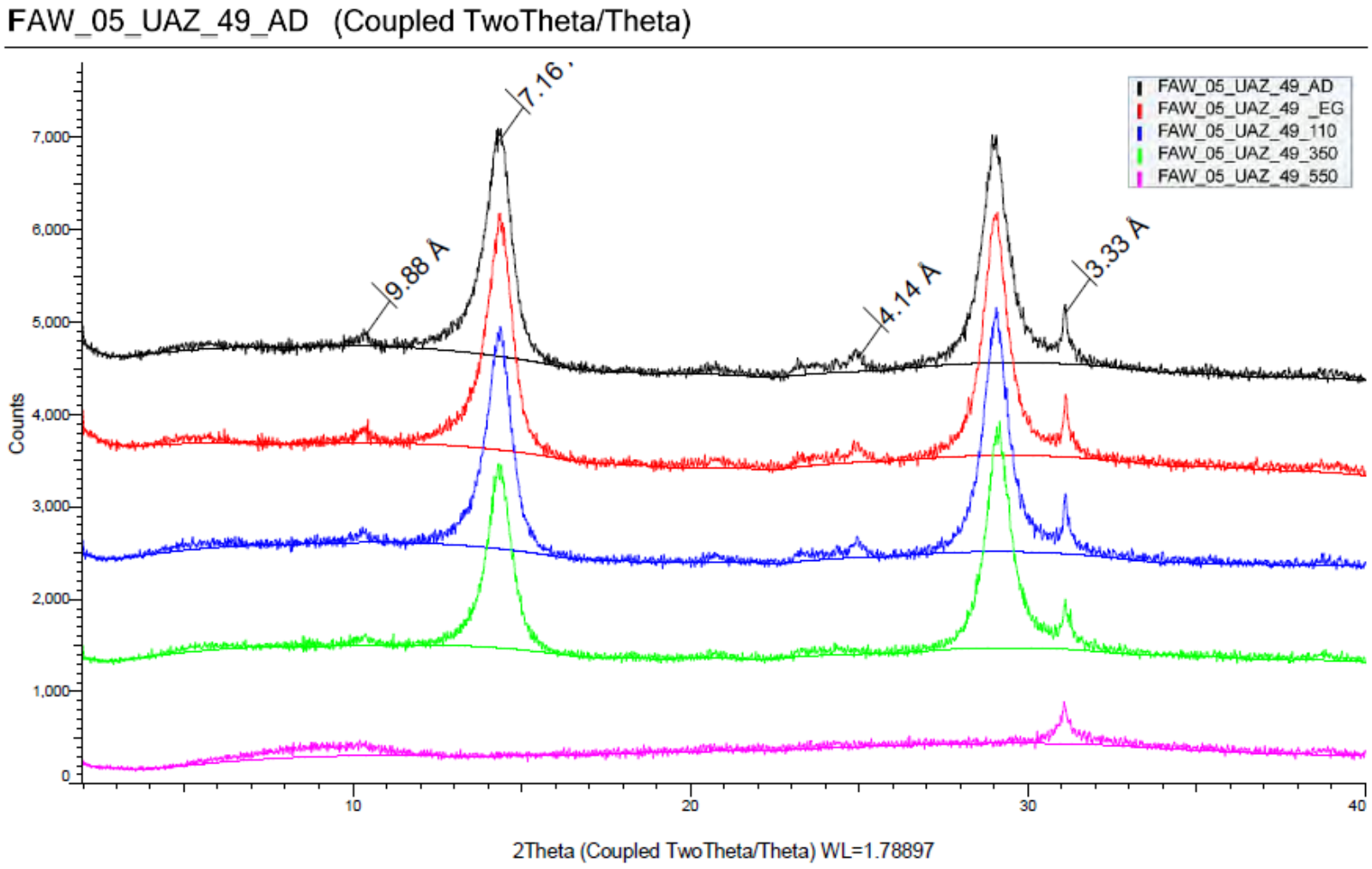

Figure 6-4. Clay fraction XRD diffraction pattern: FAW-05, UAZ, 49 ft

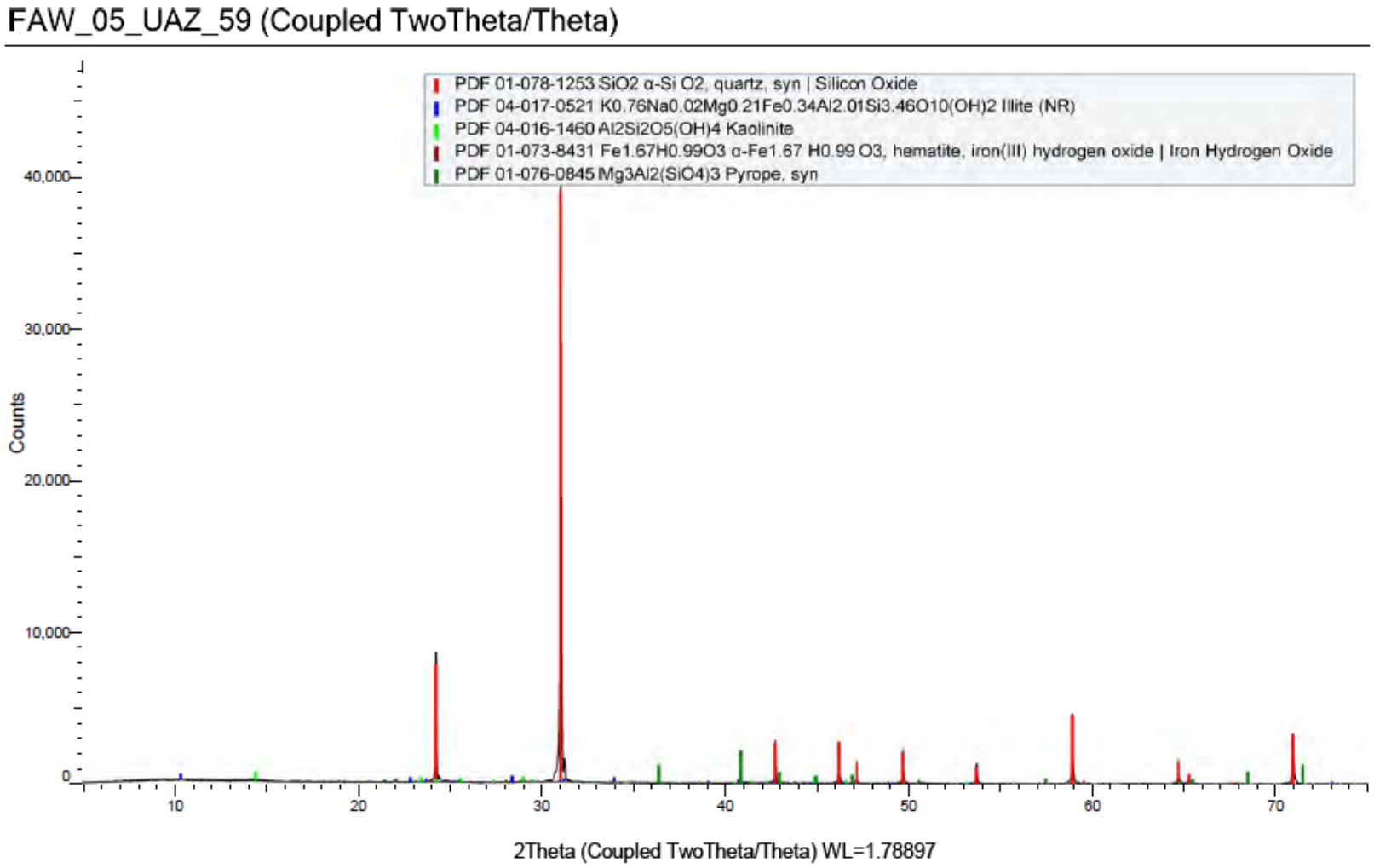

Figure 6-5. Bulk XRD diffraction pattern: FAW-05, UAZ, 59 ft

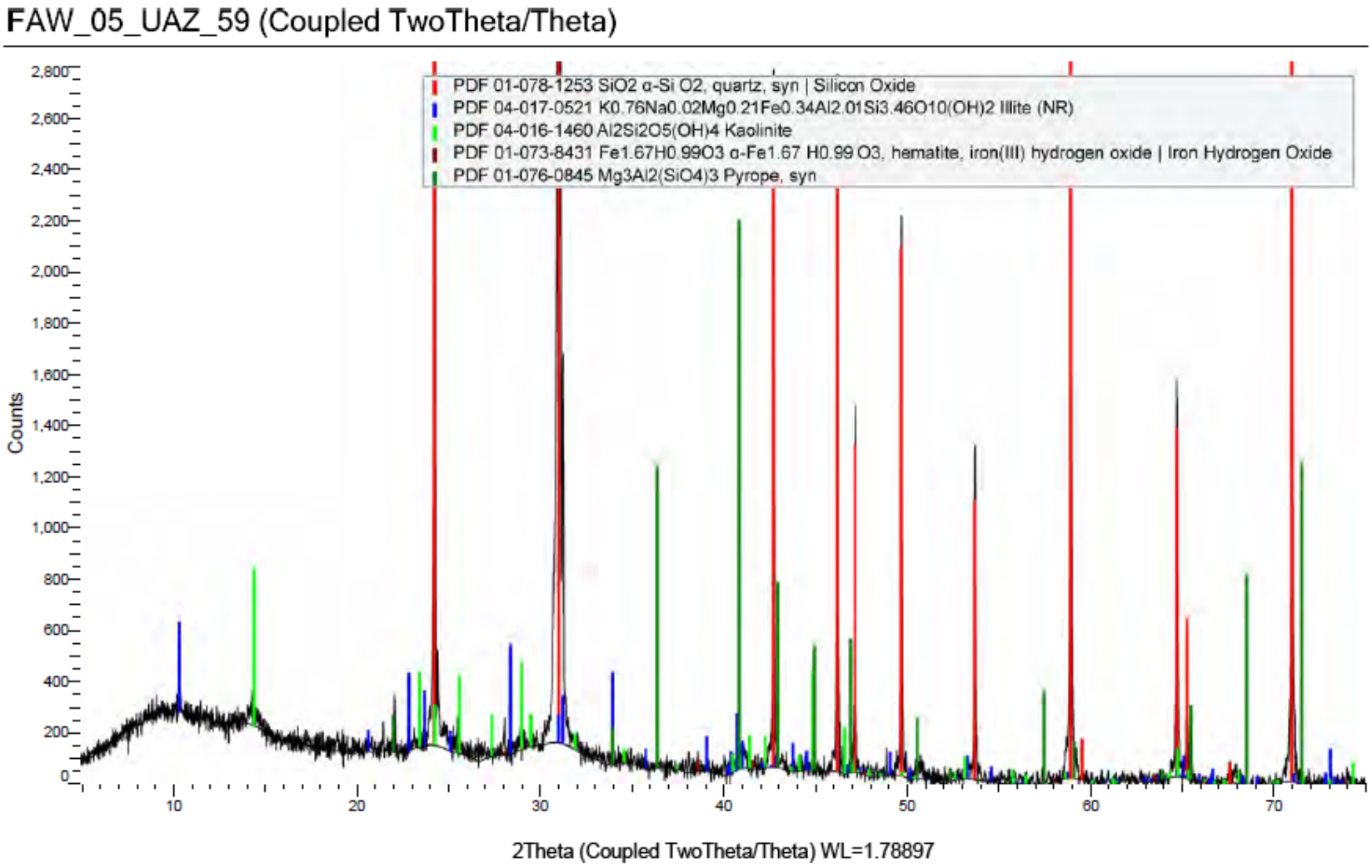

Figure 6-6. Zoomed bulk XRD diffraction pattern: FAW-05, UAZ, 59 ft

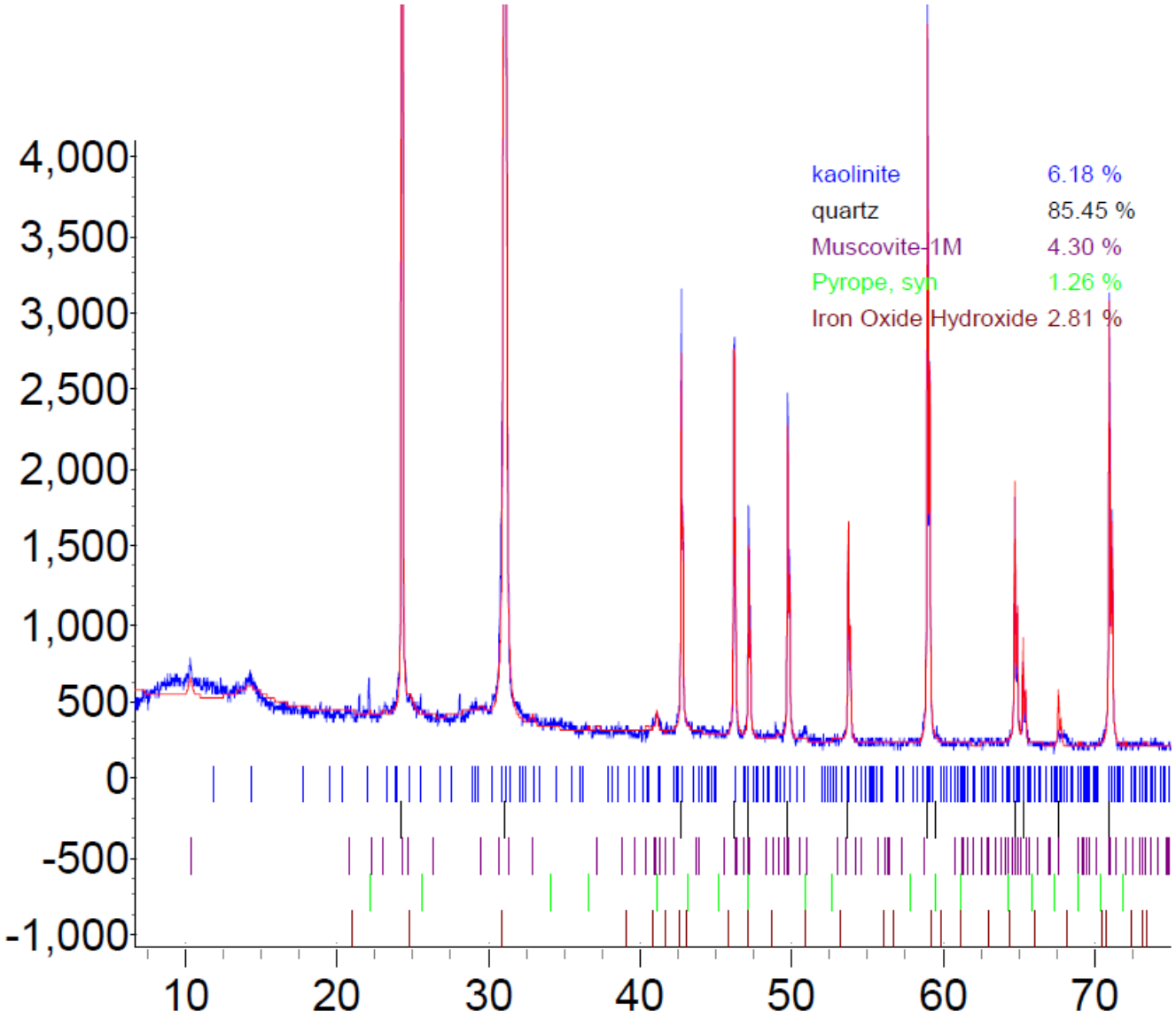

Figure 6-7. Bulk XRD identification and semi-quantification: FAW-05, UAZ, 59 ft

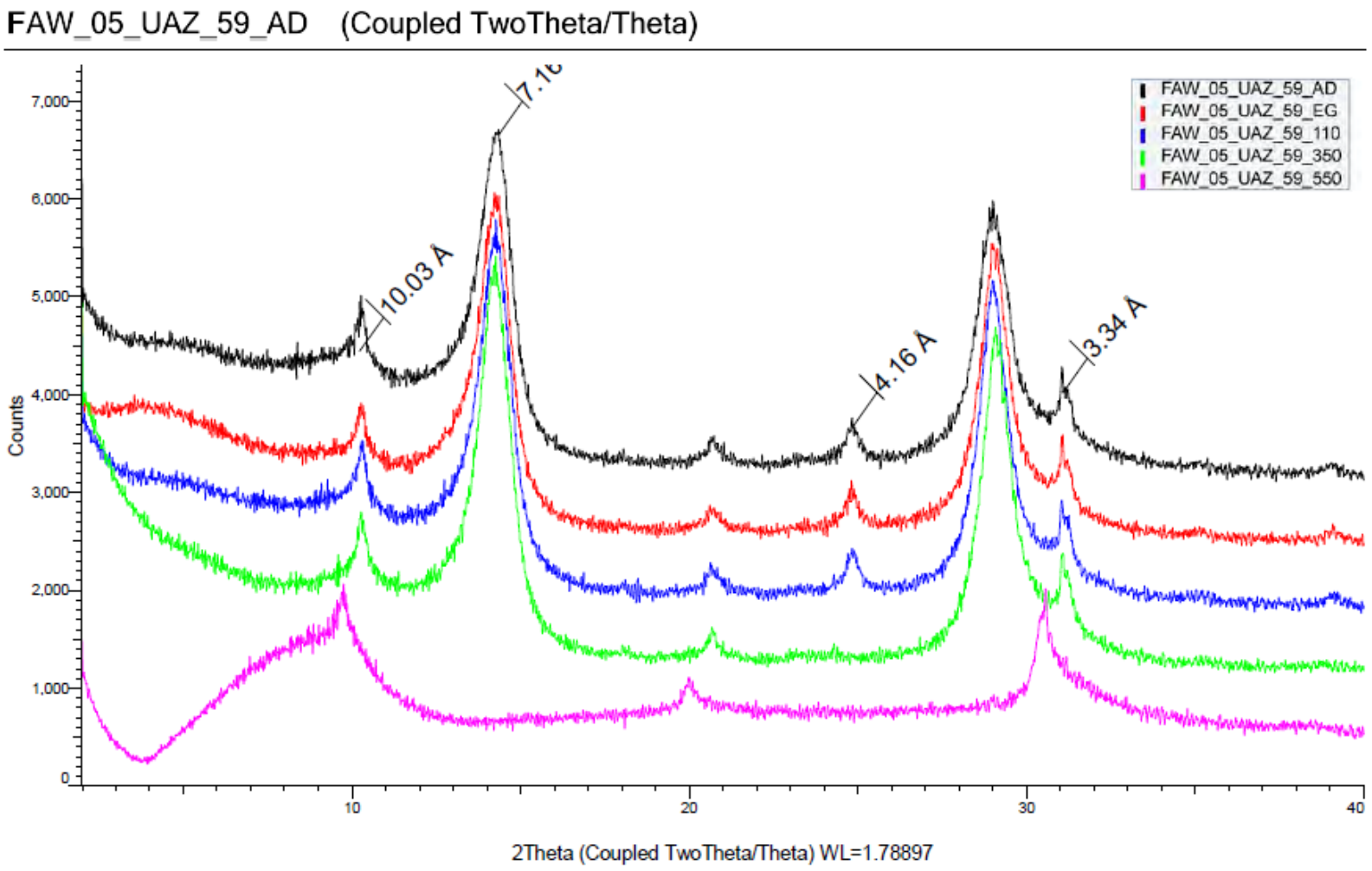

Figure 6-8. Clay fraction XRD diffraction pattern: FAW-05, UAZ, 59 ft

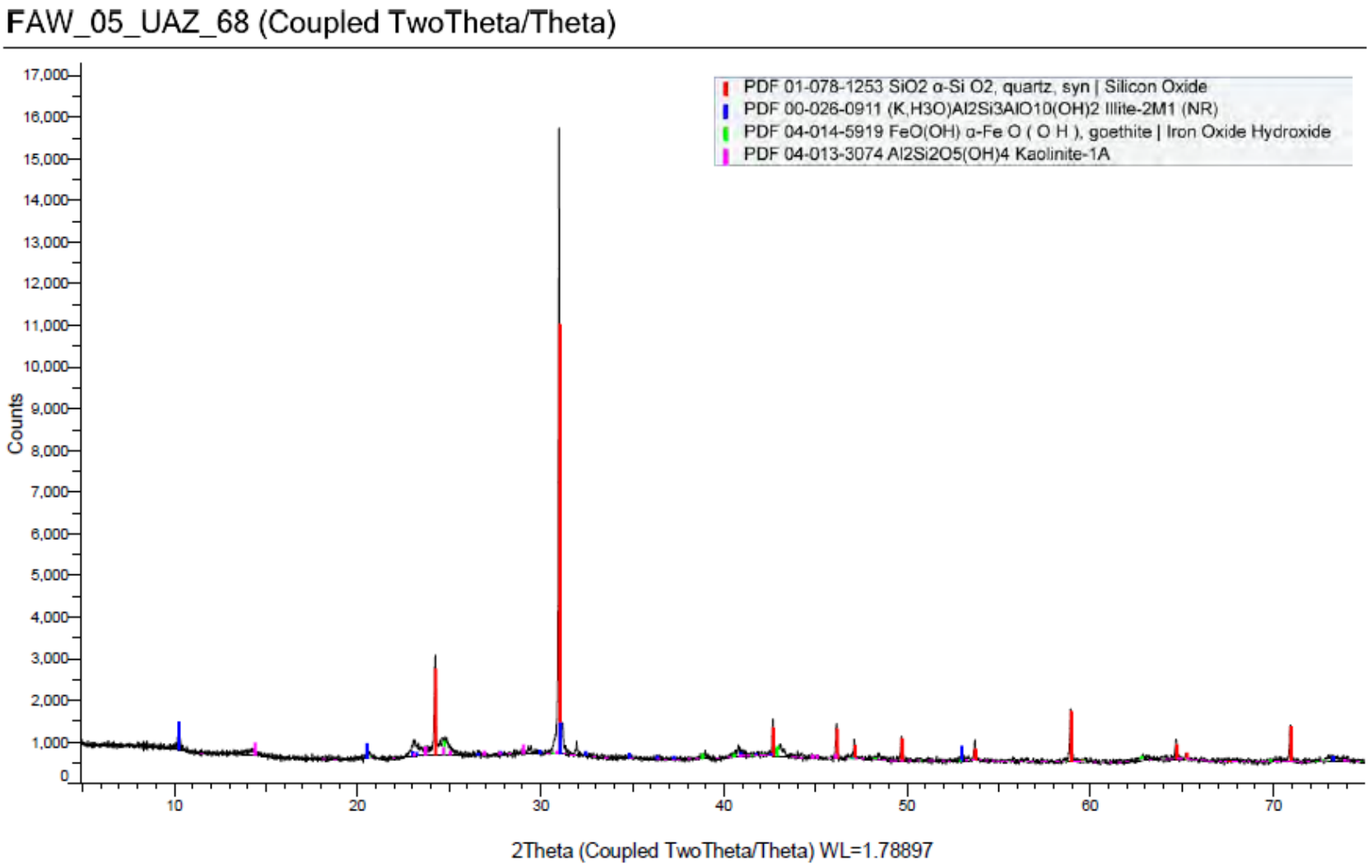

Figure 6-9. Bulk XRD diffraction pattern: FAW-05, UAZ, 68 ft

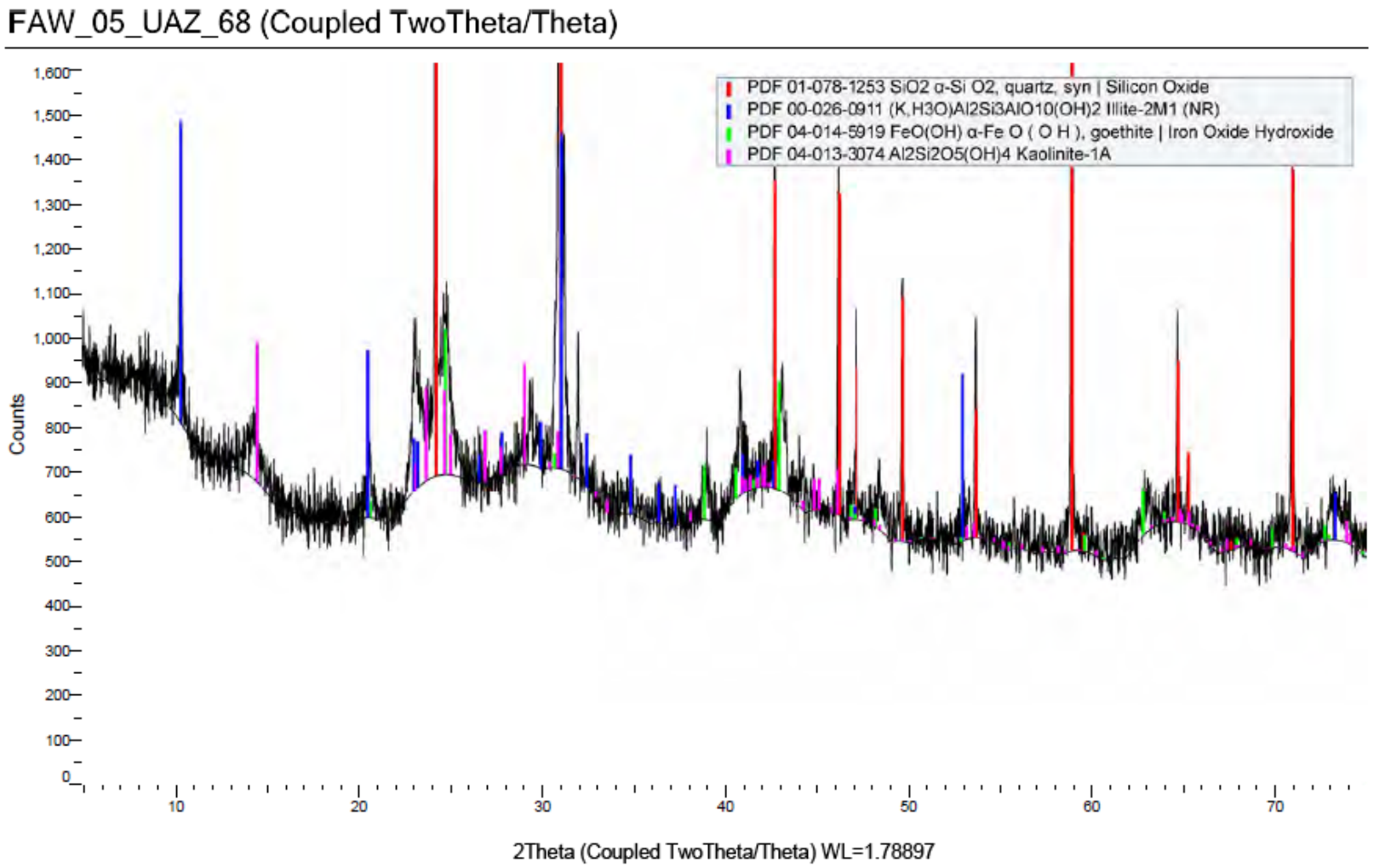

Figure 6-10. Zoomed bulk XRD diffraction pattern: FAW-05, UAZ, 68 ft

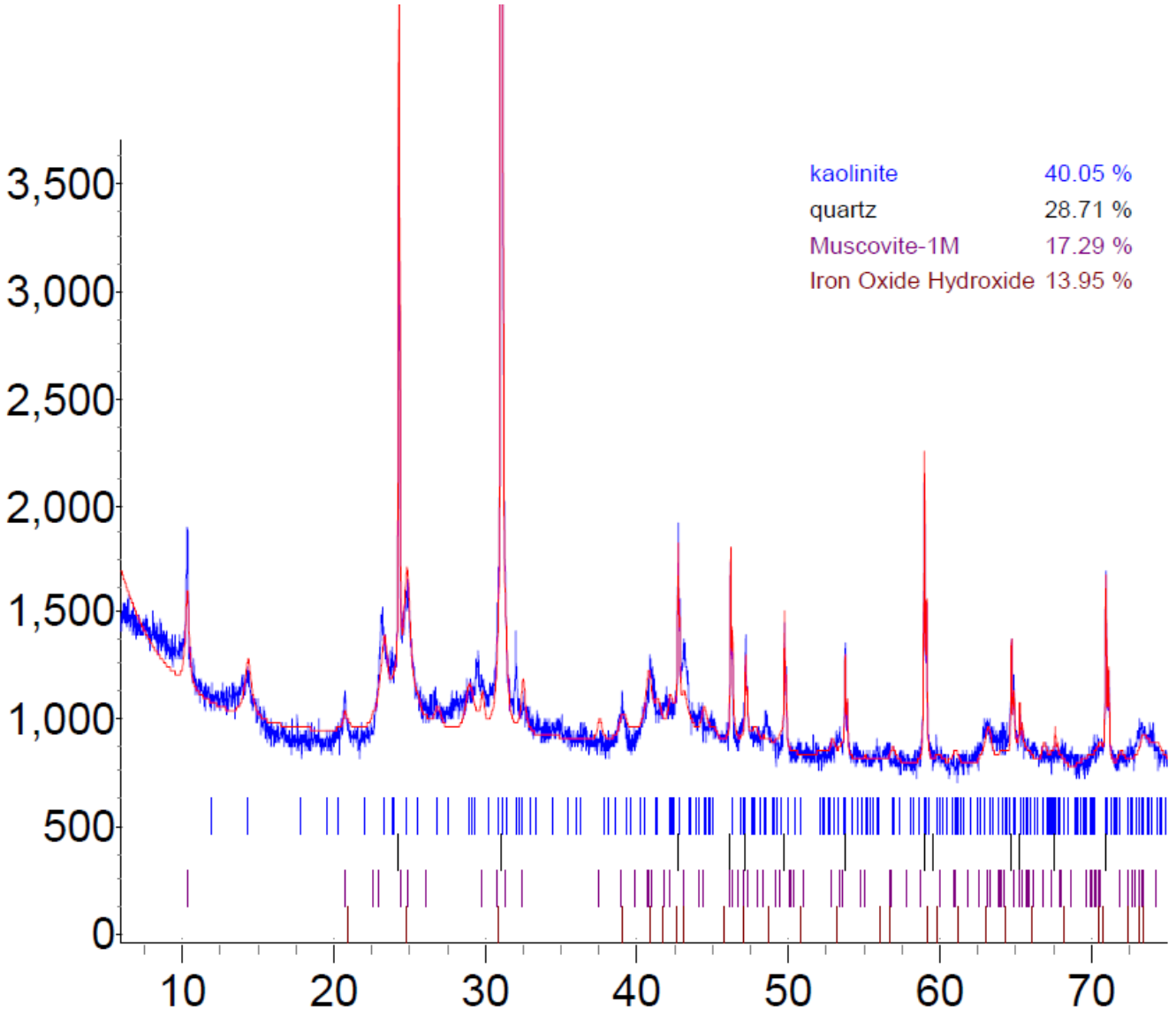

Figure 6-11. Bulk XRD identification and semi-quantification: FAW-05, UAZ, 68 ft

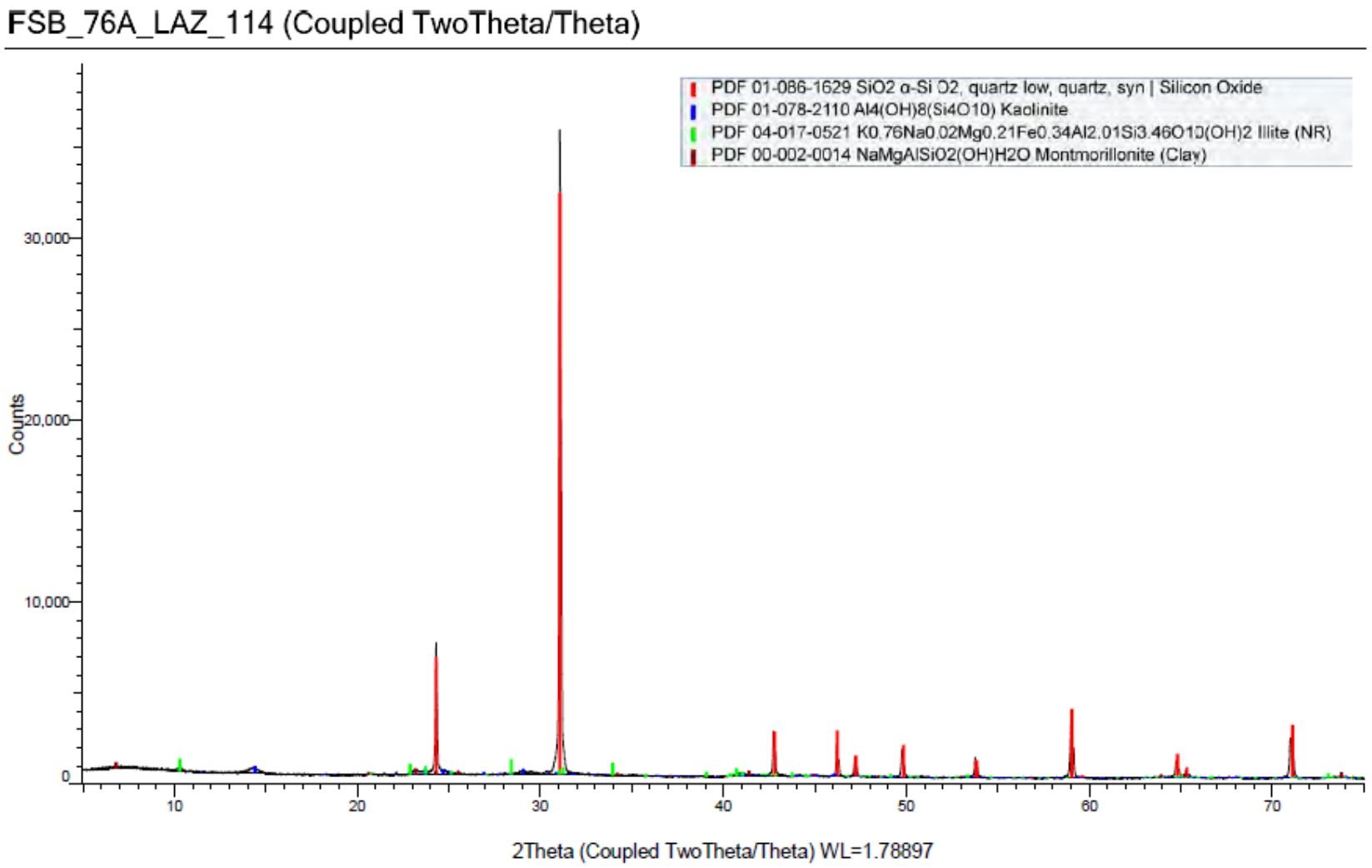

Figure 6-12. Bulk XRD diffraction pattern: FSB-76A, LAZ, 114 ft

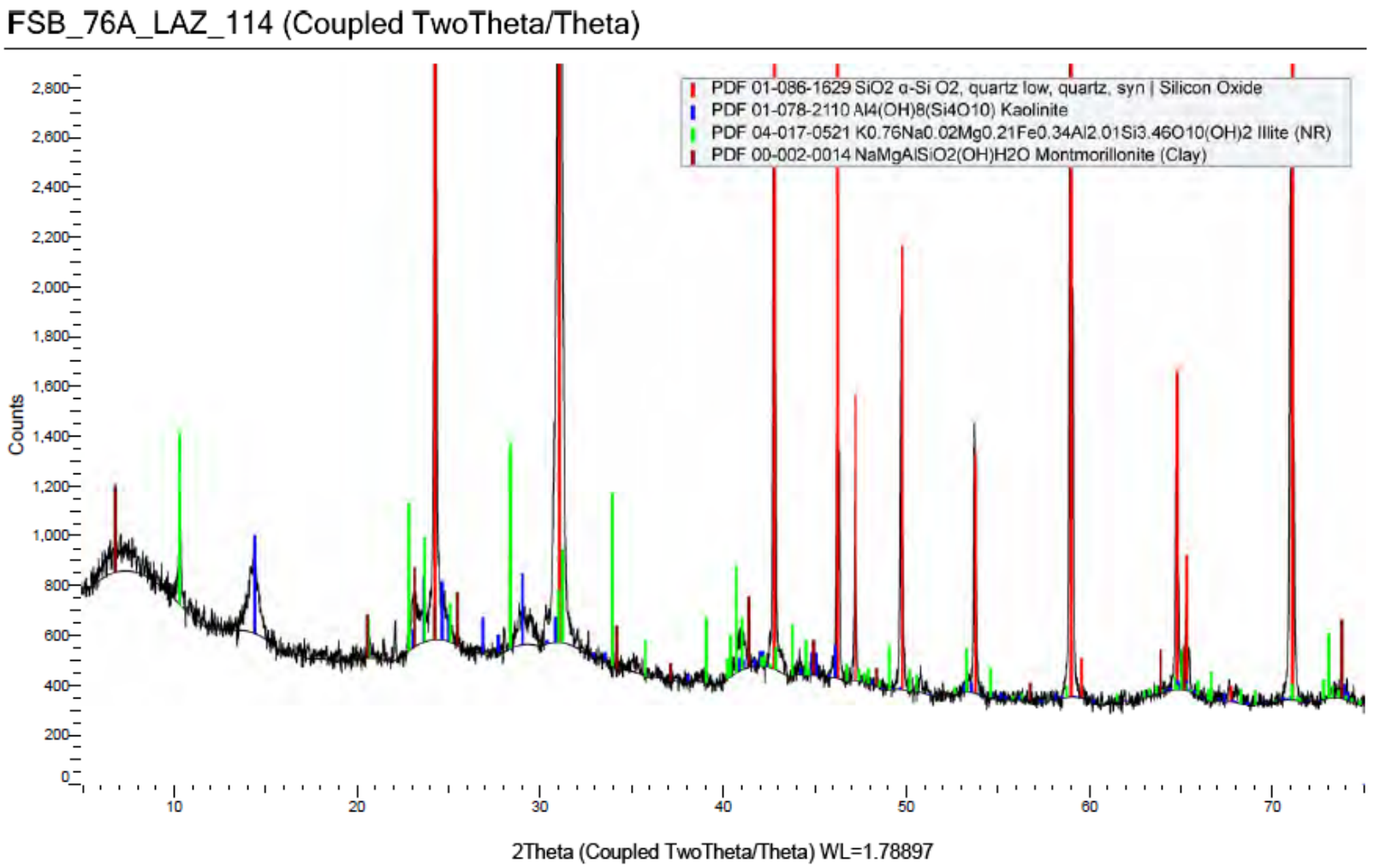

Figure 6-13. Zoomed bulk XRD diffraction pattern: FSB-76A, LAZ, 114 ft

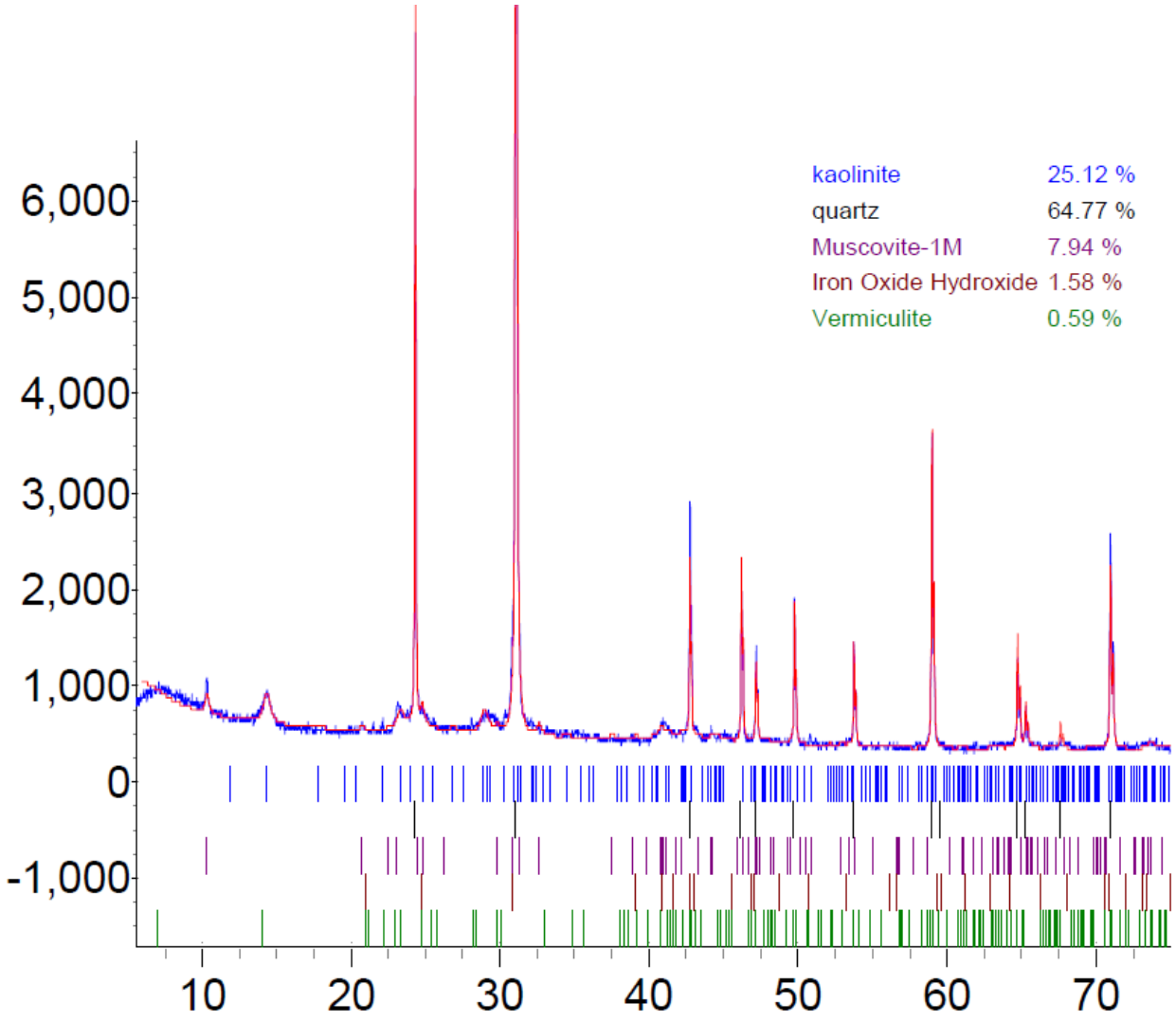

Figure 6-14. Bulk XRD identification and semi-quantification: FSB-76A, LAZ, 114 ft

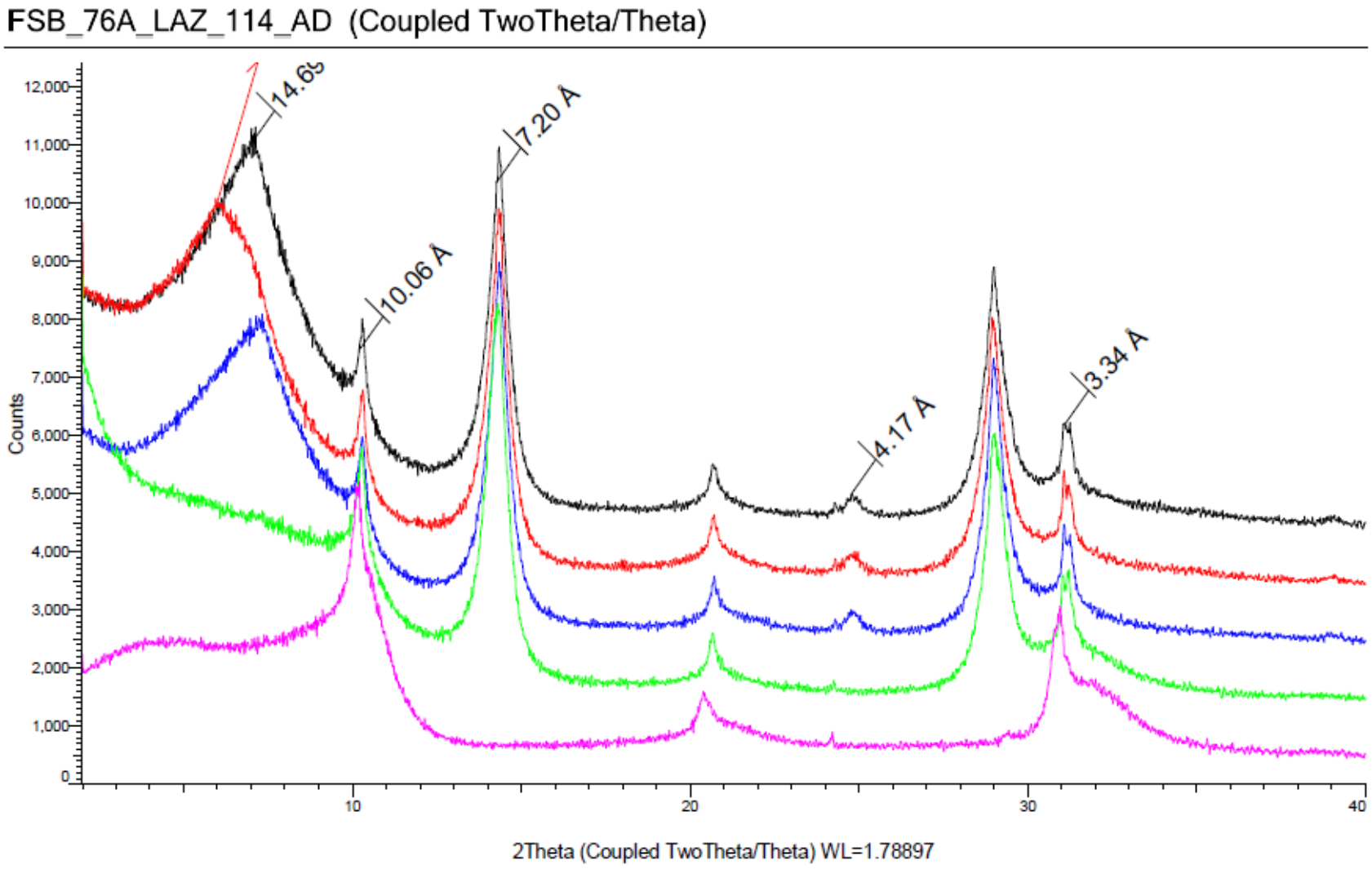

Figure 6-15. Clay fraction XRD diffraction pattern: FSB-76A, LAZ, 114 ft

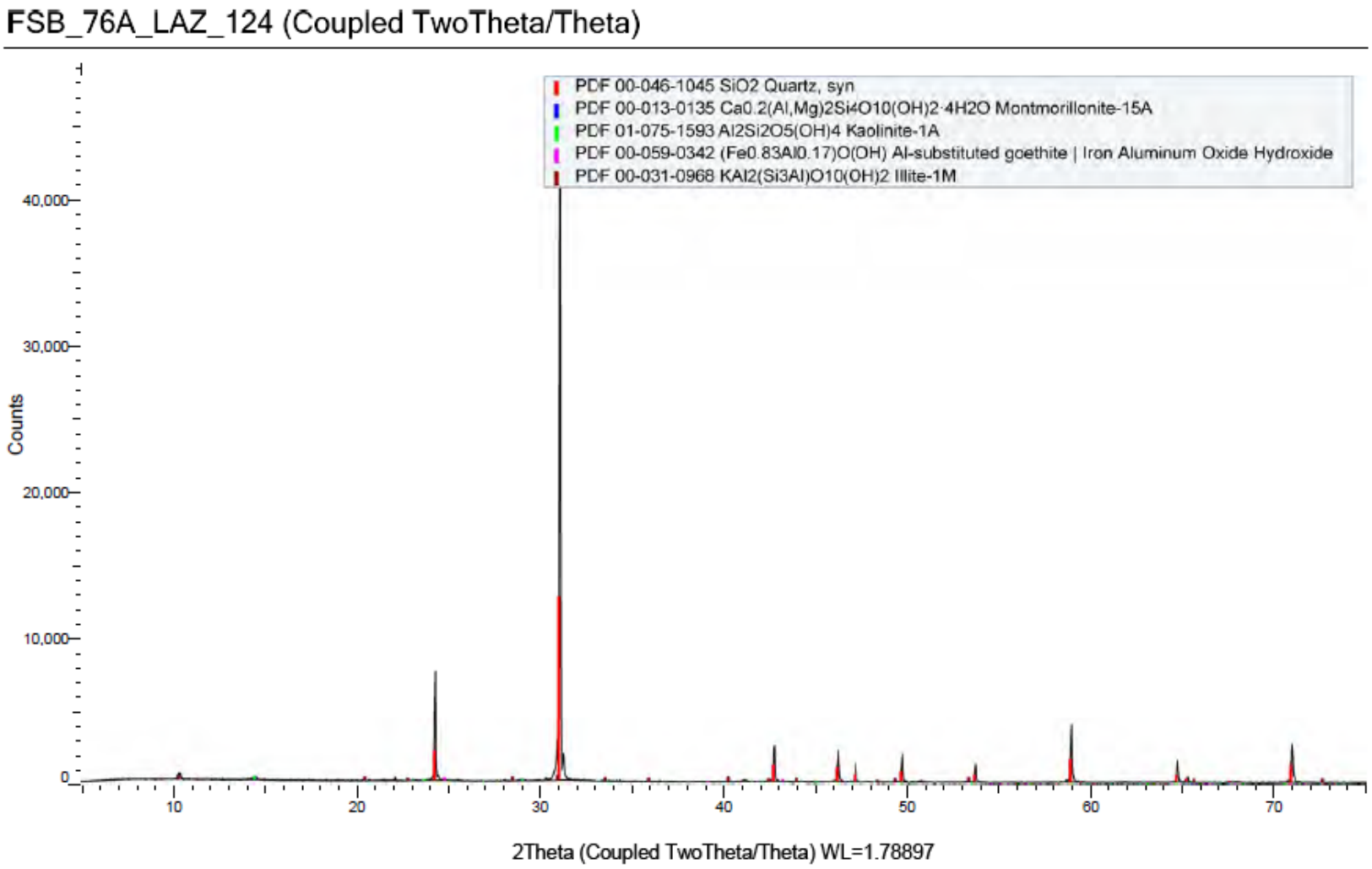

Figure 6-16. Bulk XRD diffraction pattern: FSB-76A, LAZ, 124 ft

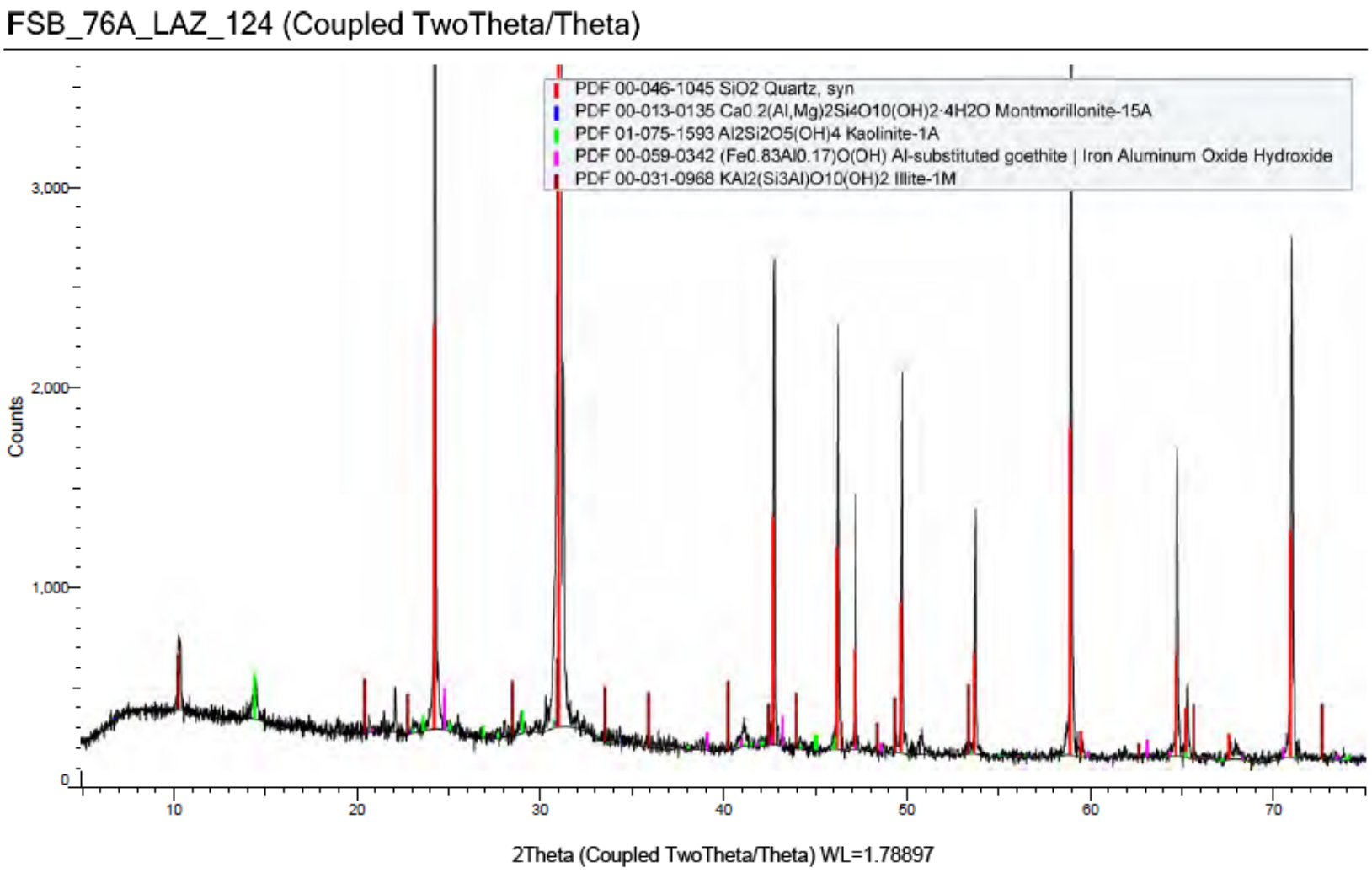

Figure 6-17. Zoomed bulk XRD diffraction pattern: FSB-76A, LAZ, 124 ft

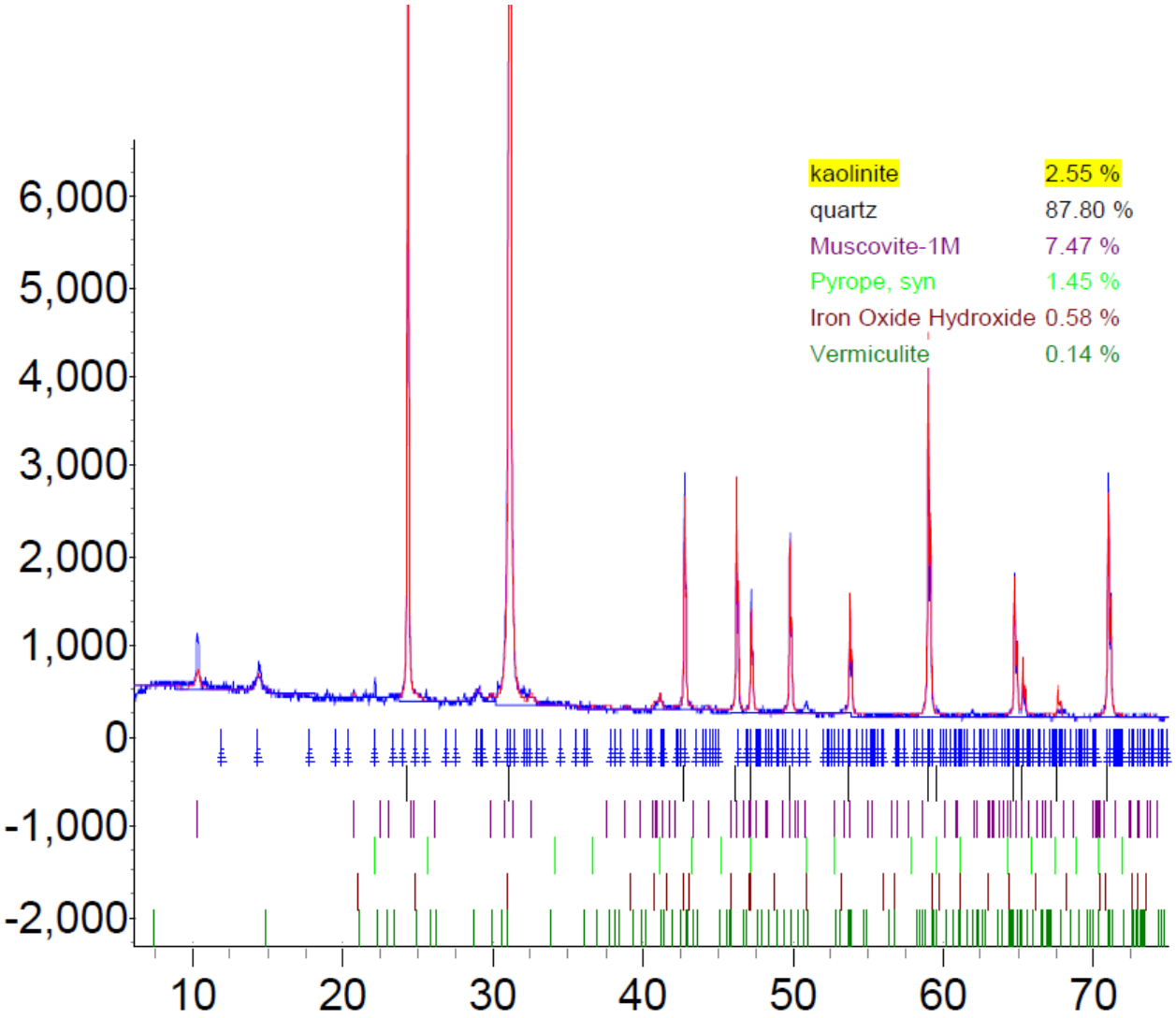

Figure 6-18. Bulk XRD identification and semi-quantification: FSB-76A, LAZ, 124 ft

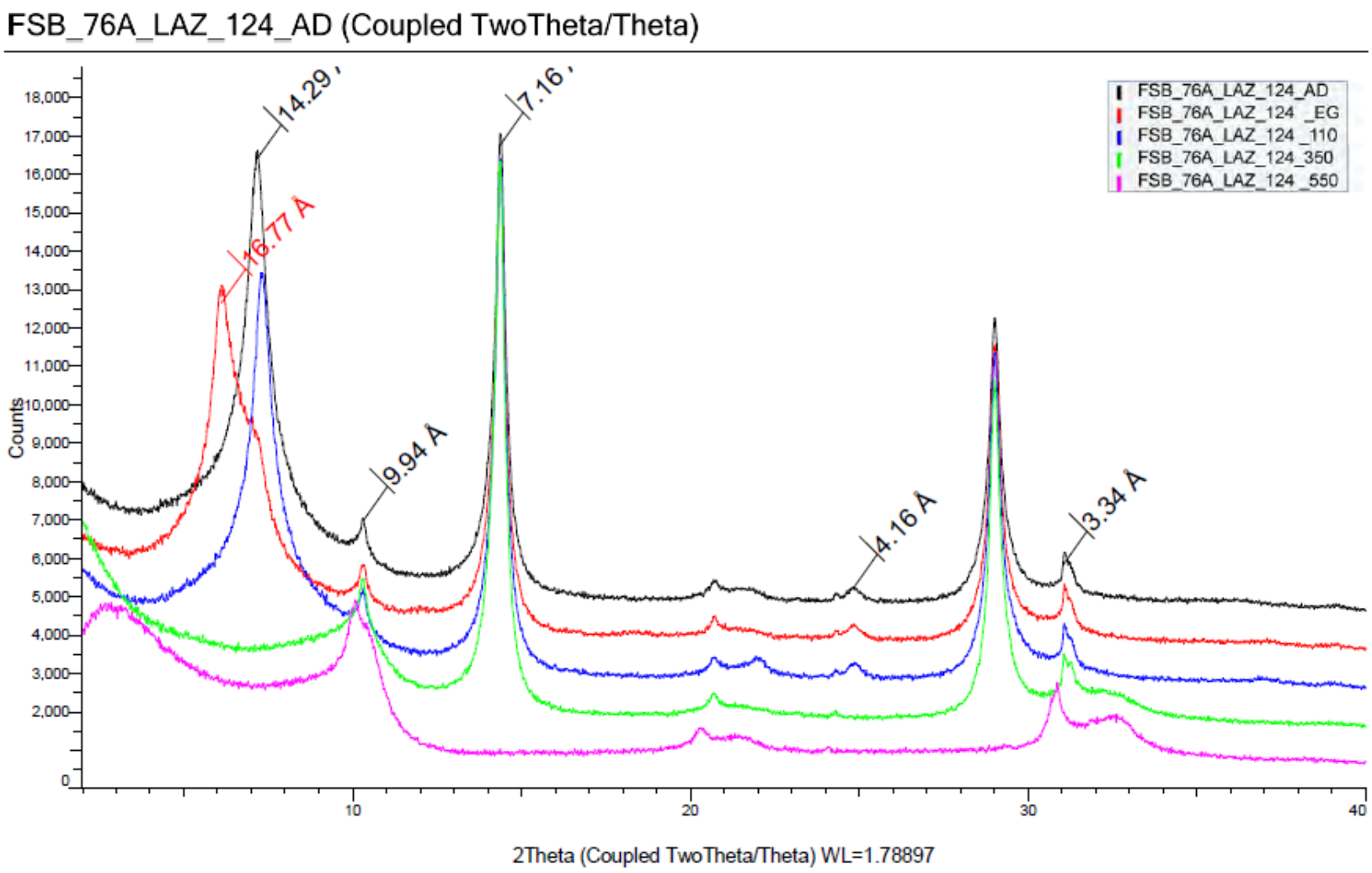

Figure 6-19. Clay fraction XRD diffraction pattern: FSB-76A, LAZ, 124 ft

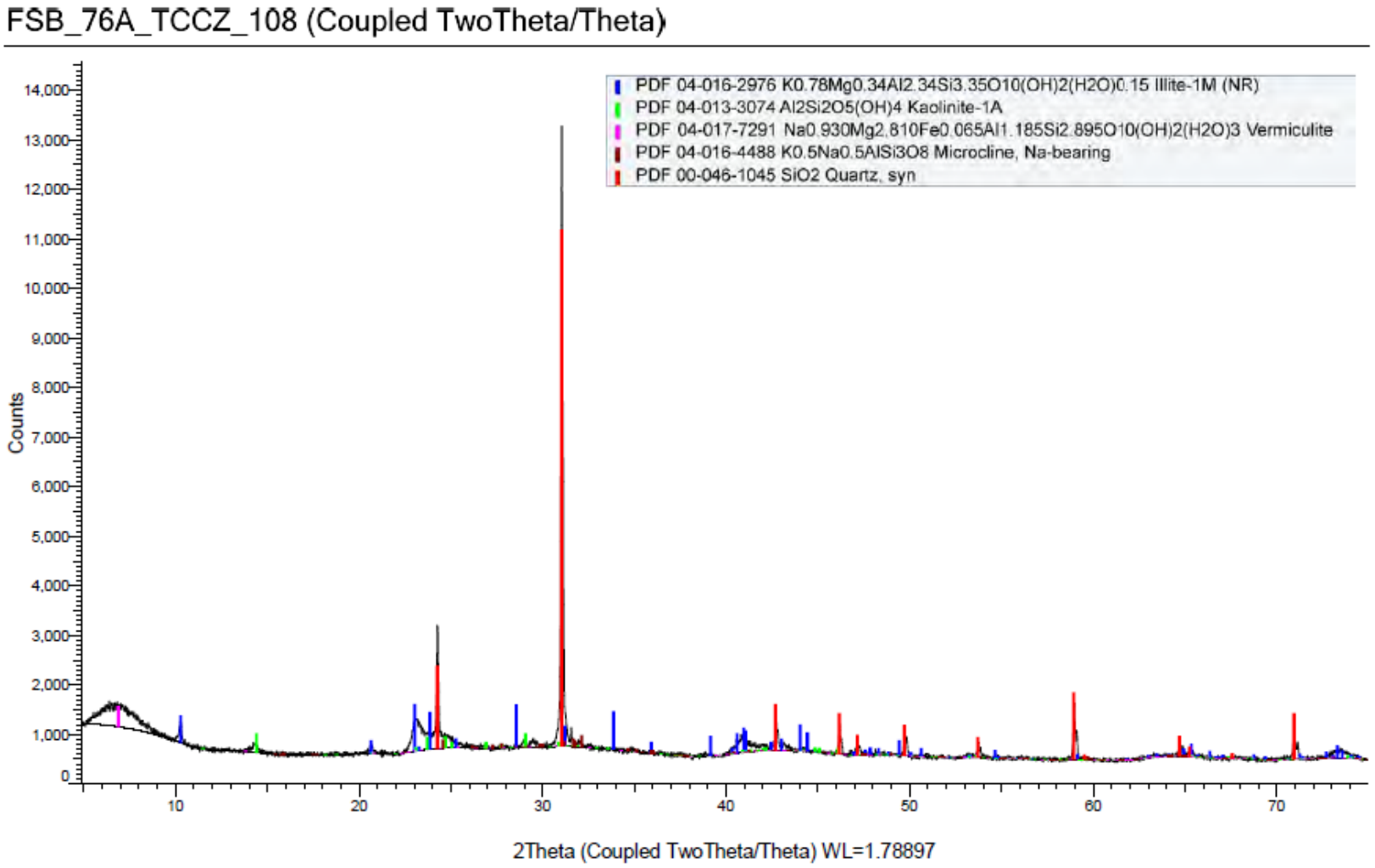

Figure 6-20. Bulk XRD diffraction pattern: FSB-76A, TCCZ, 108 ft

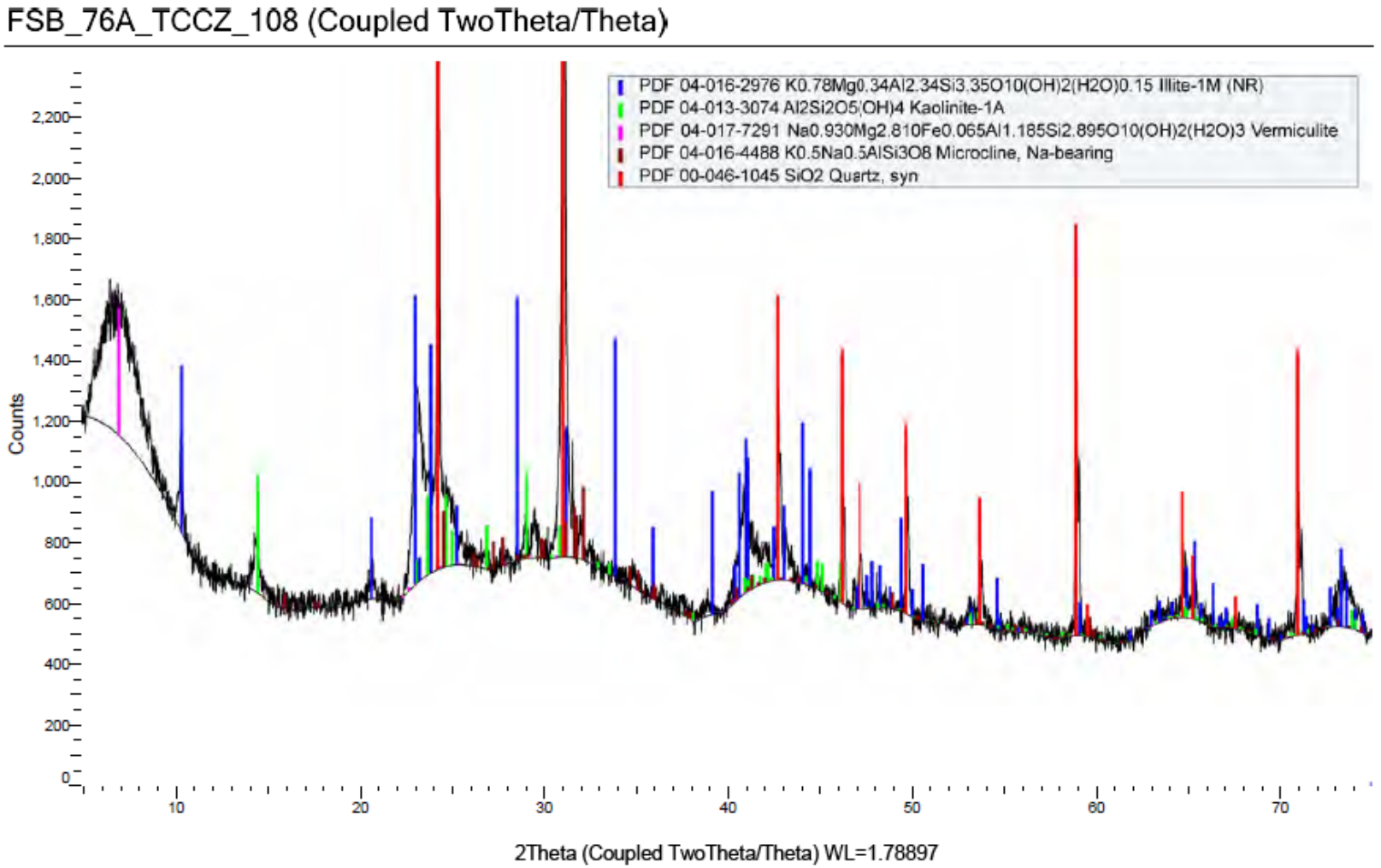

Figure 6-21. Zoomed bulk XRD diffraction pattern: FSB-76A, TCCZ, 108 ft

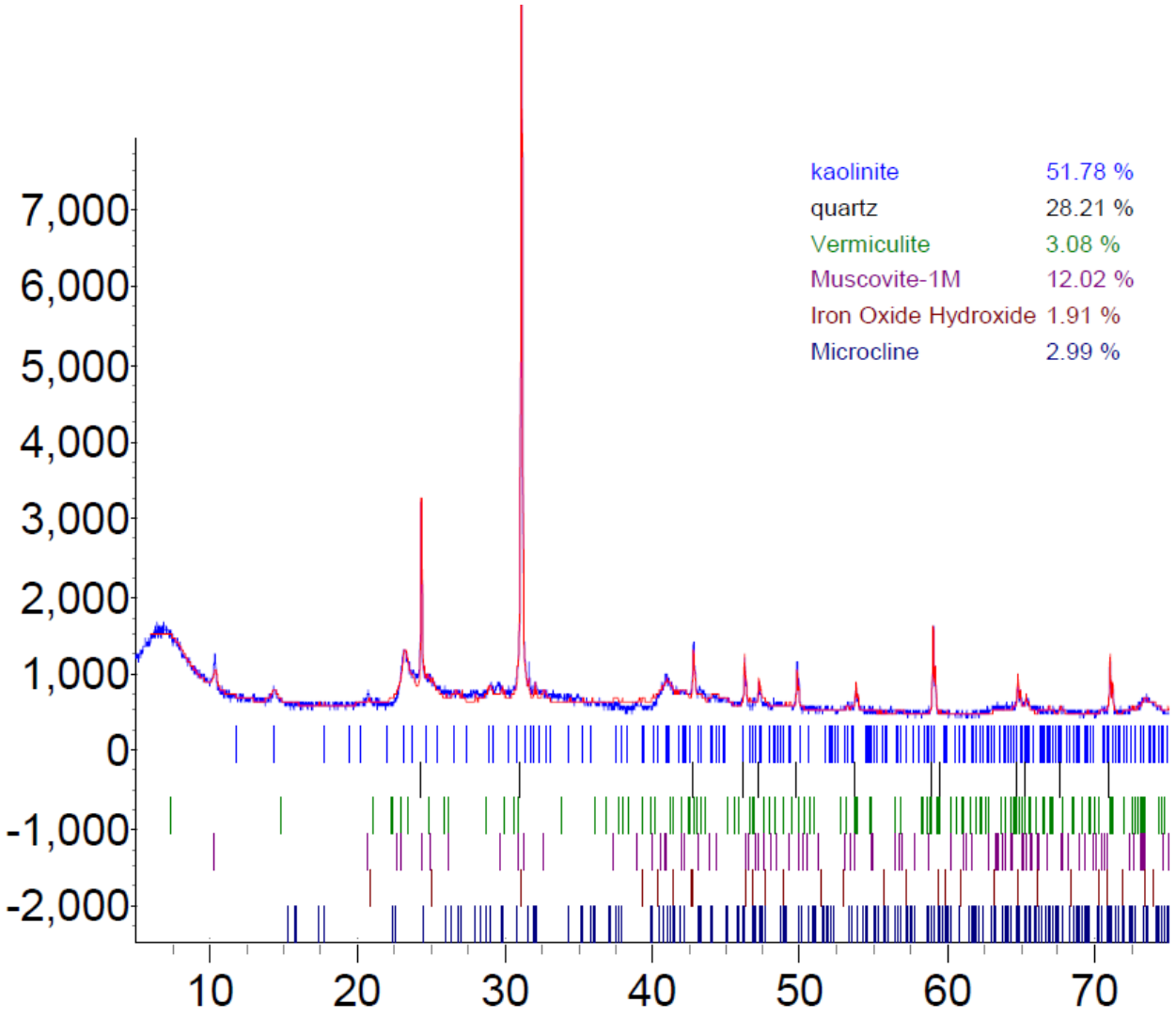

Figure 6-22. Bulk XRD identification and semi-quantification: FSB-76A, TCCZ, 108 ft

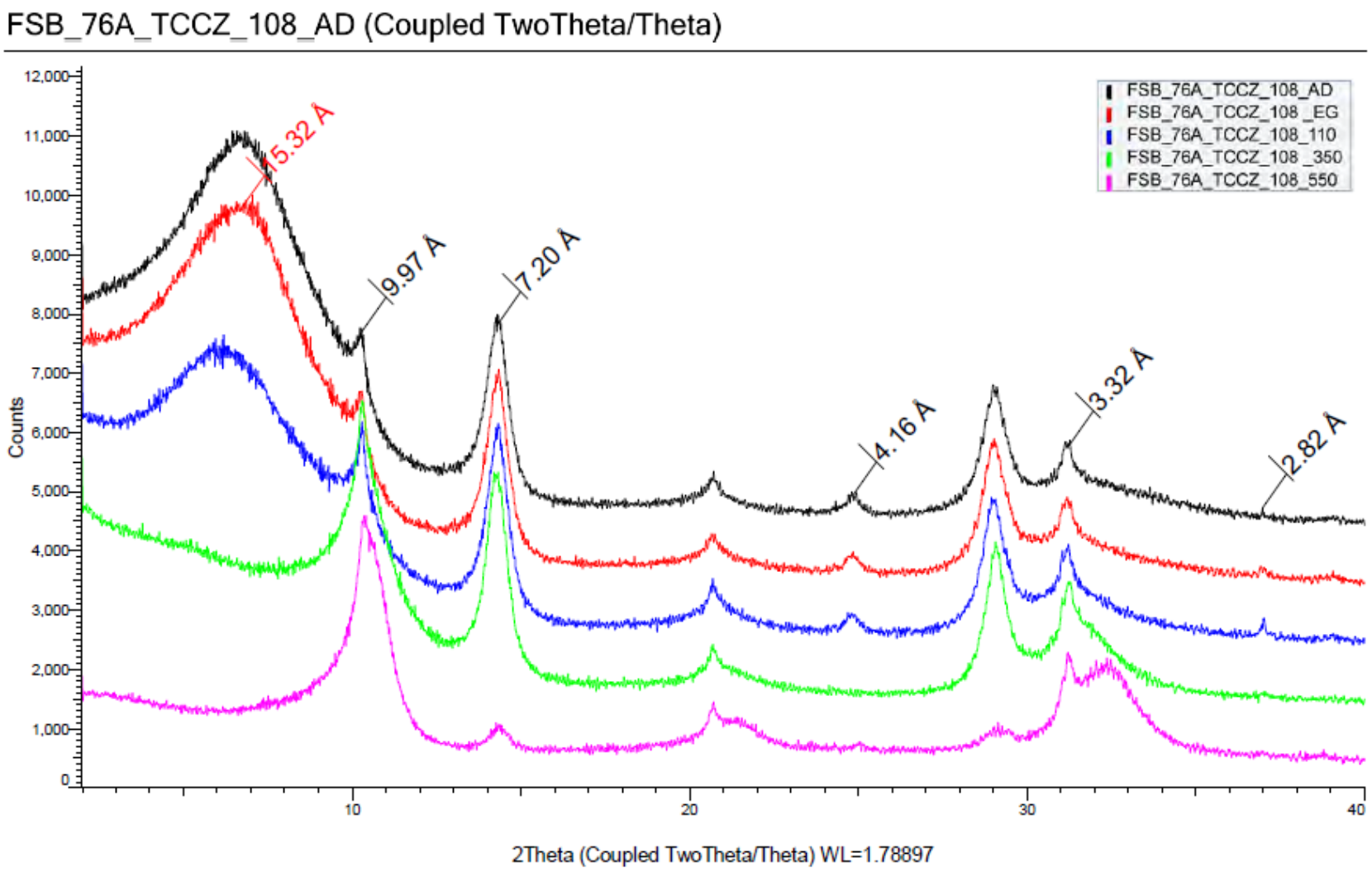

Figure 6-23. Clay fraction XRD diffraction pattern: FSB-76A, TCCZ, 108 ft

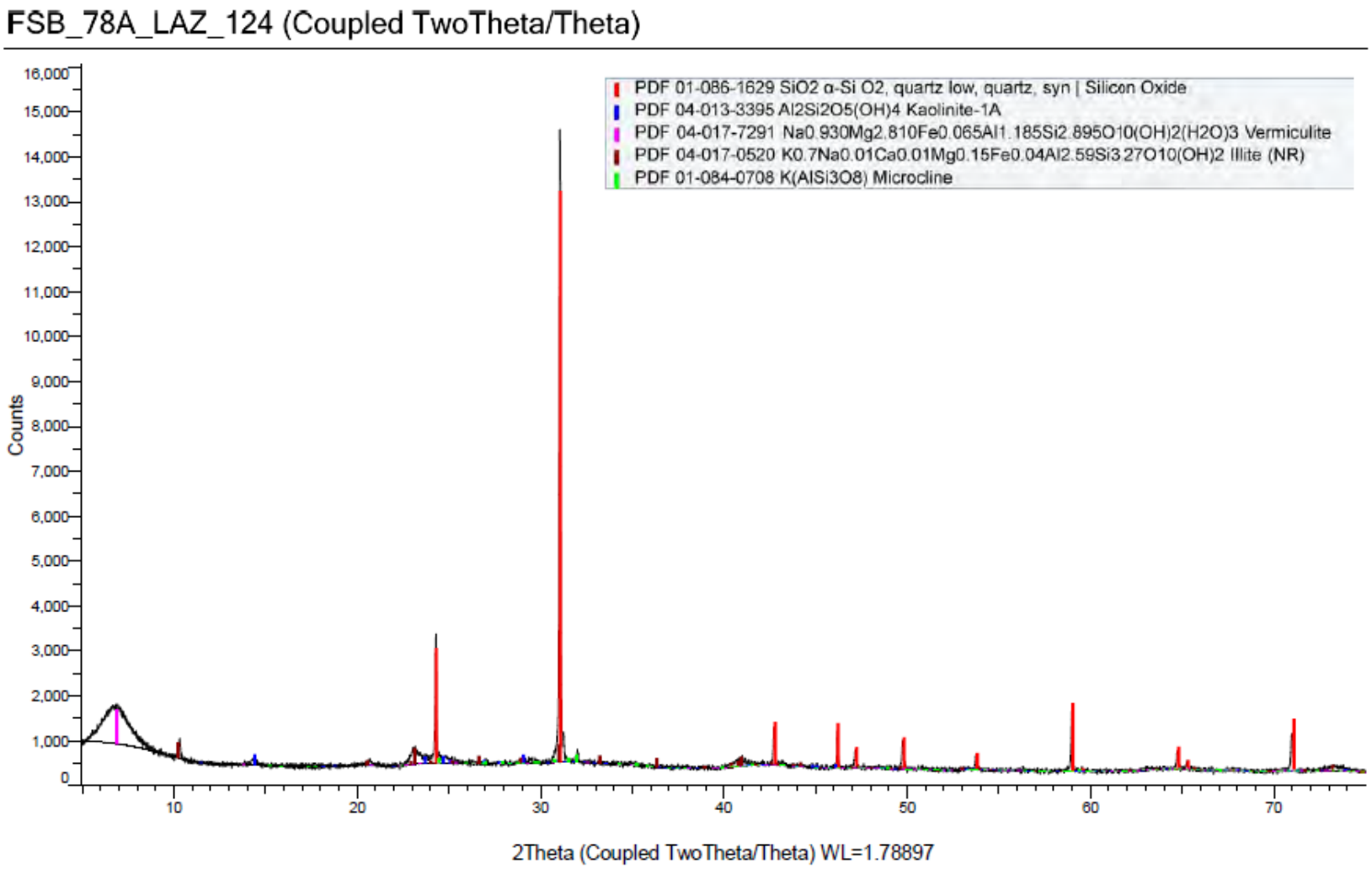

Figure 6-24. Bulk XRD diffraction pattern: FSB-78A, LAZ, 124 ft

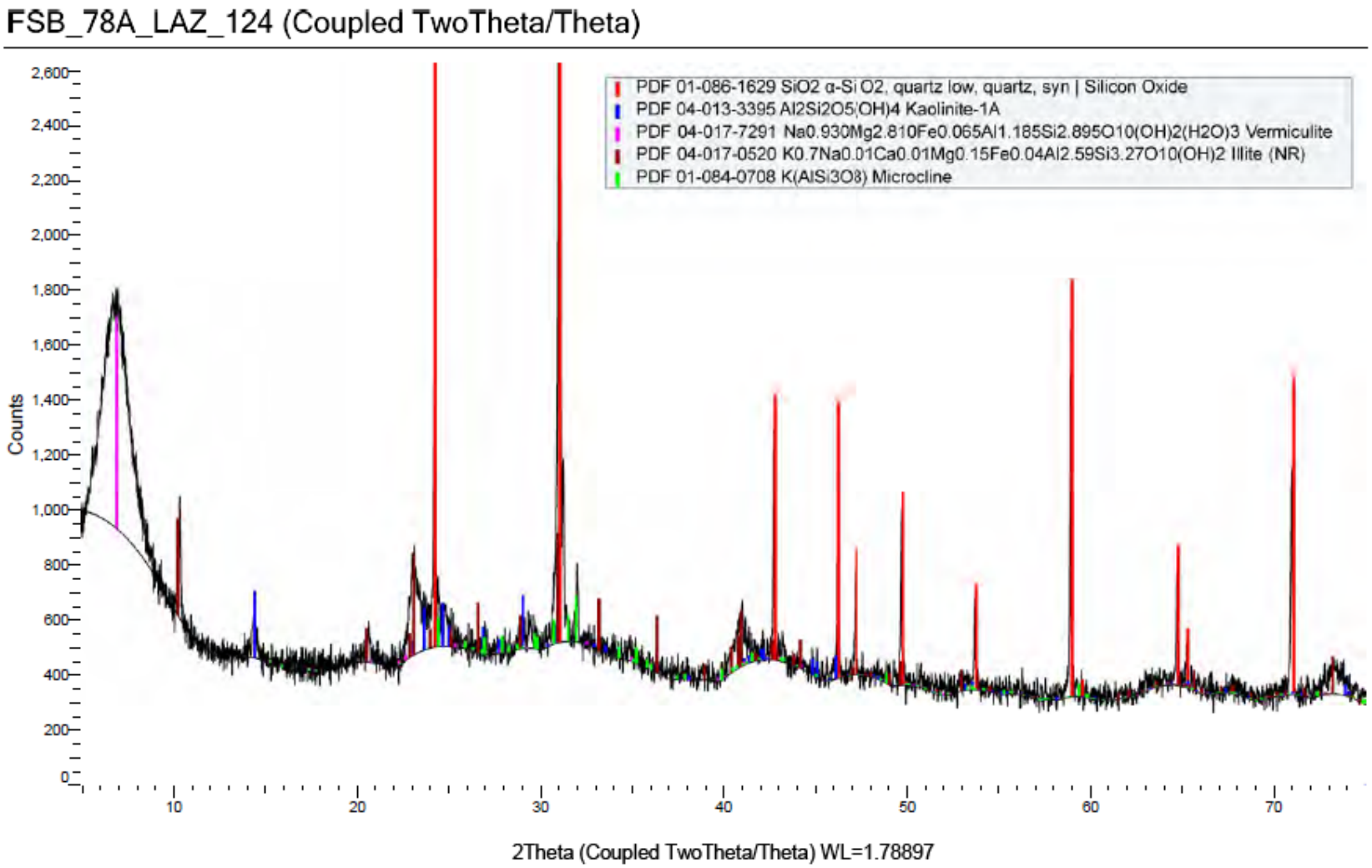

Figure 6-25. Zoomed bulk XRD diffraction pattern: FSB-78A, LAZ, 124 ft

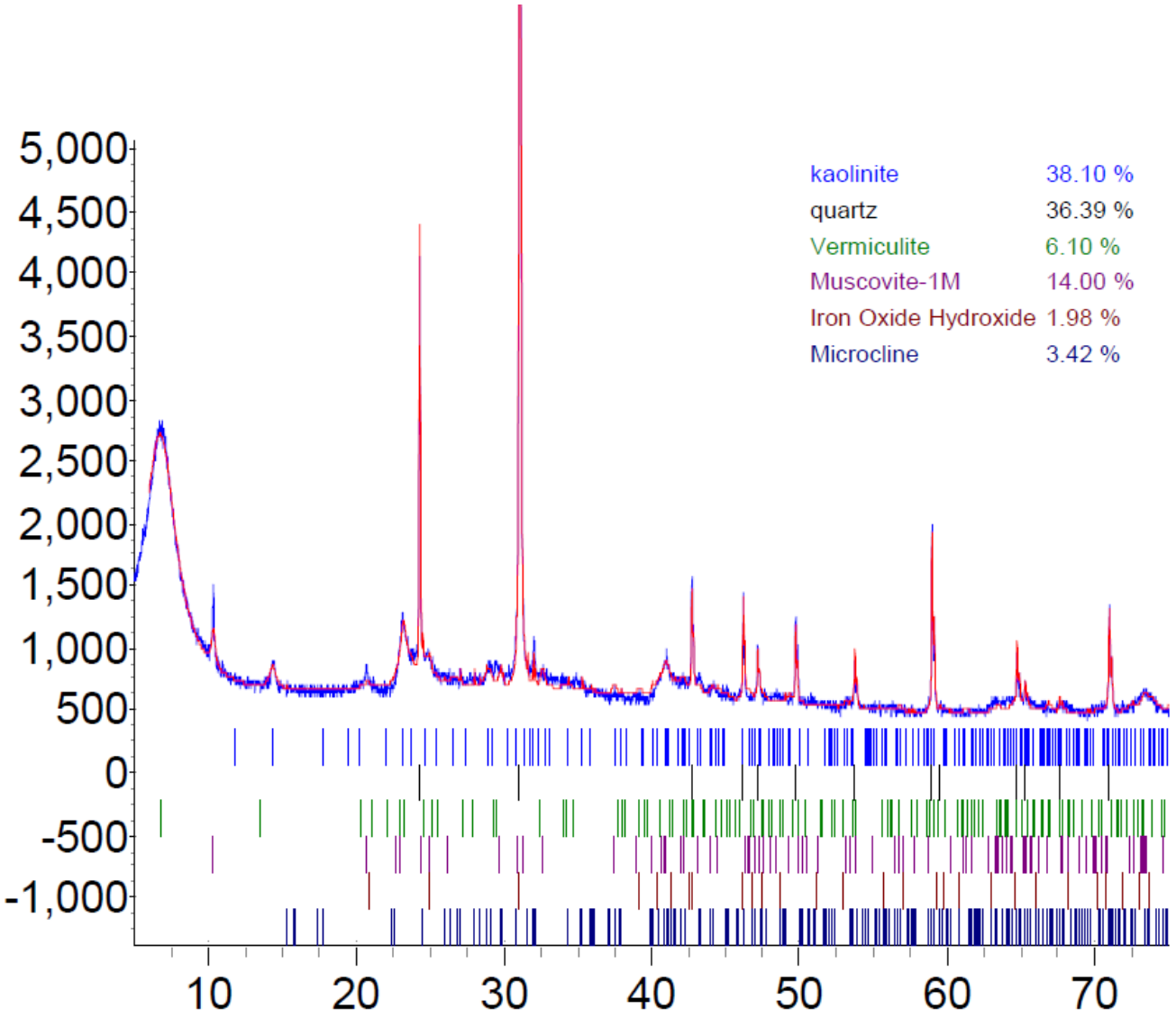

Figure 6-26. Bulk XRD identification and semi-quantification: FSB-78A, LAZ, 124 ft

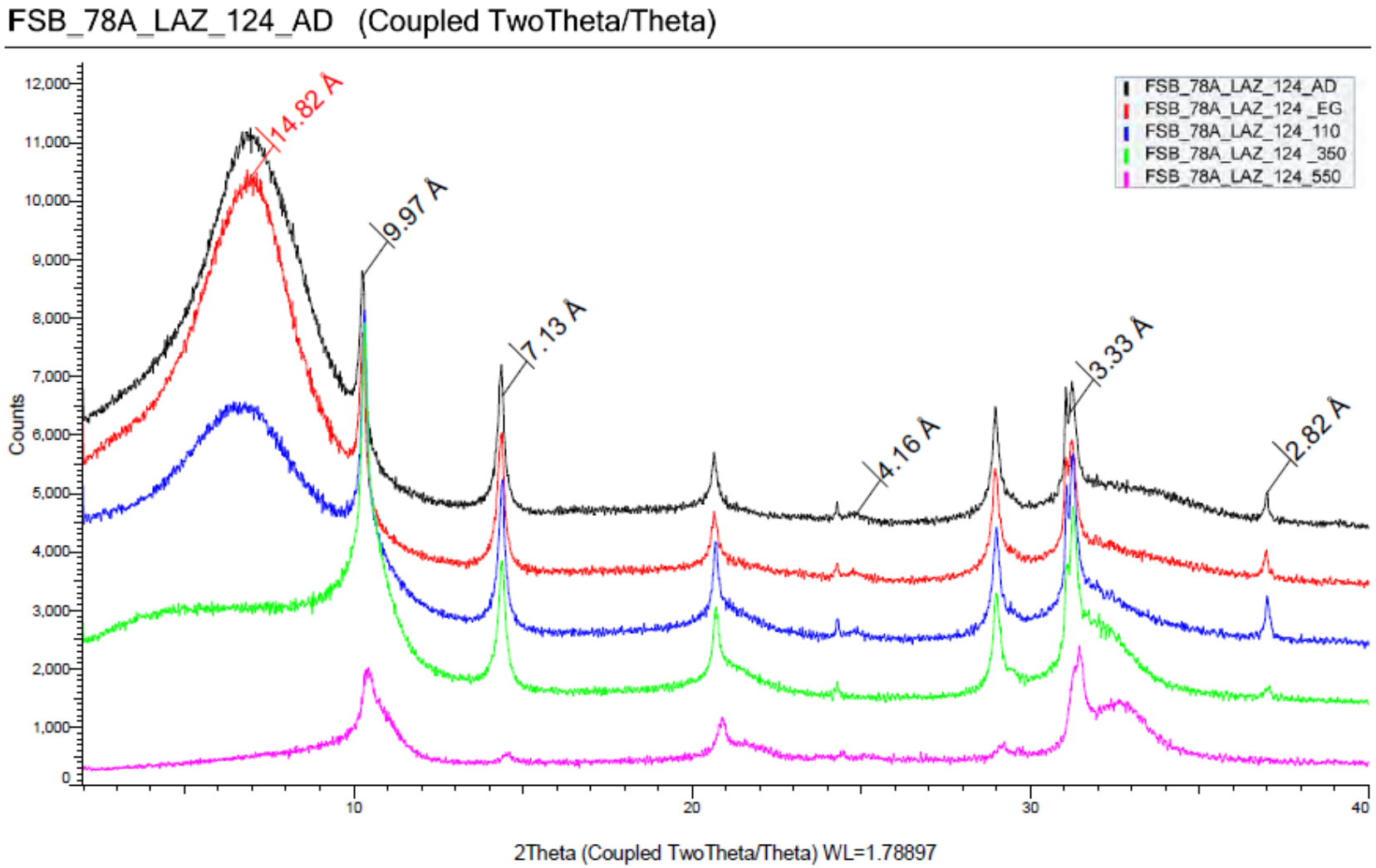

Figure 6-27. Clay fraction XRD diffraction pattern: FSB-78A, LAZ, 124 ft

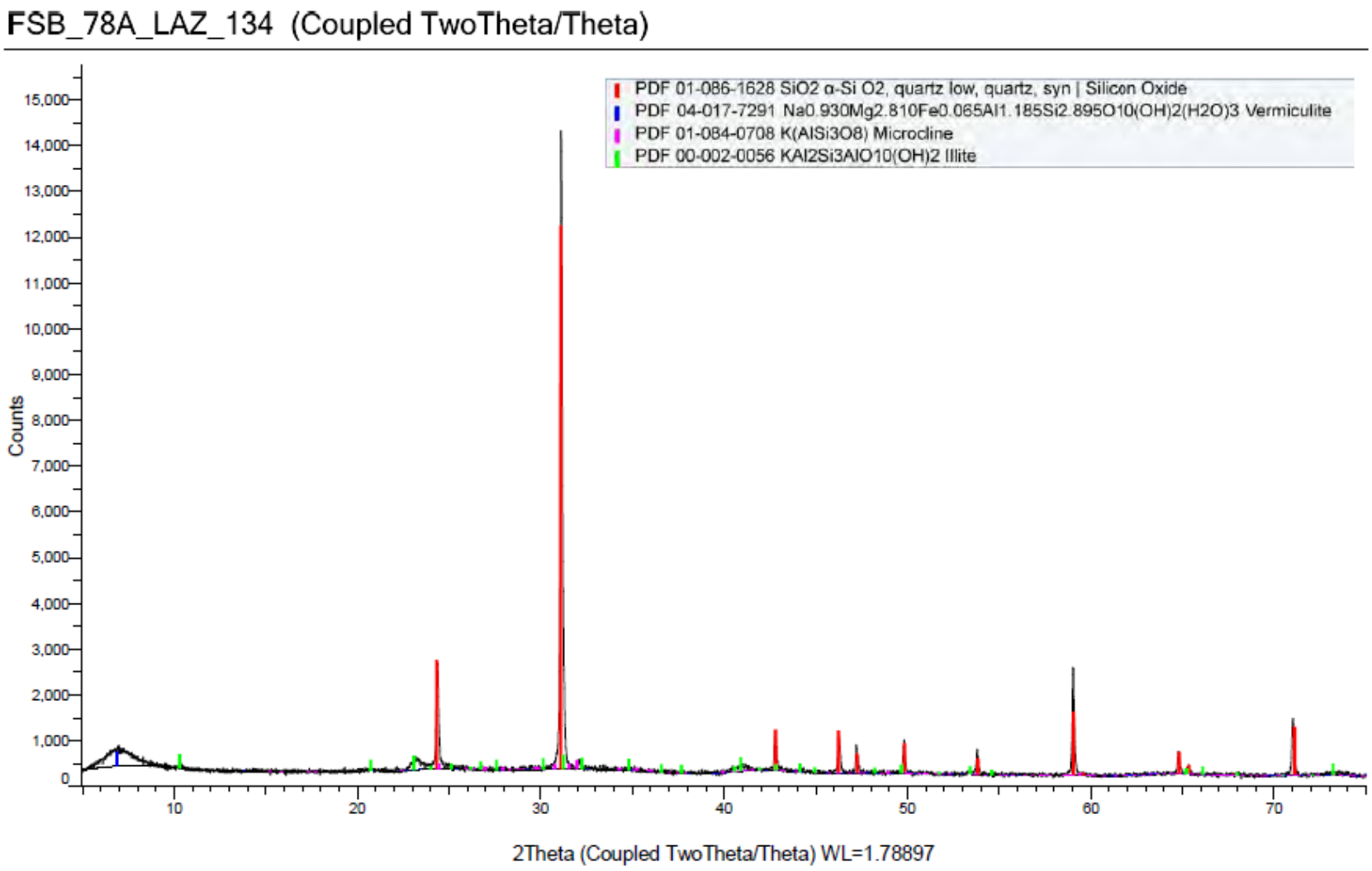

Figure 6-28. Bulk XRD diffraction pattern: FSB-78A, LAZ, 134 ft

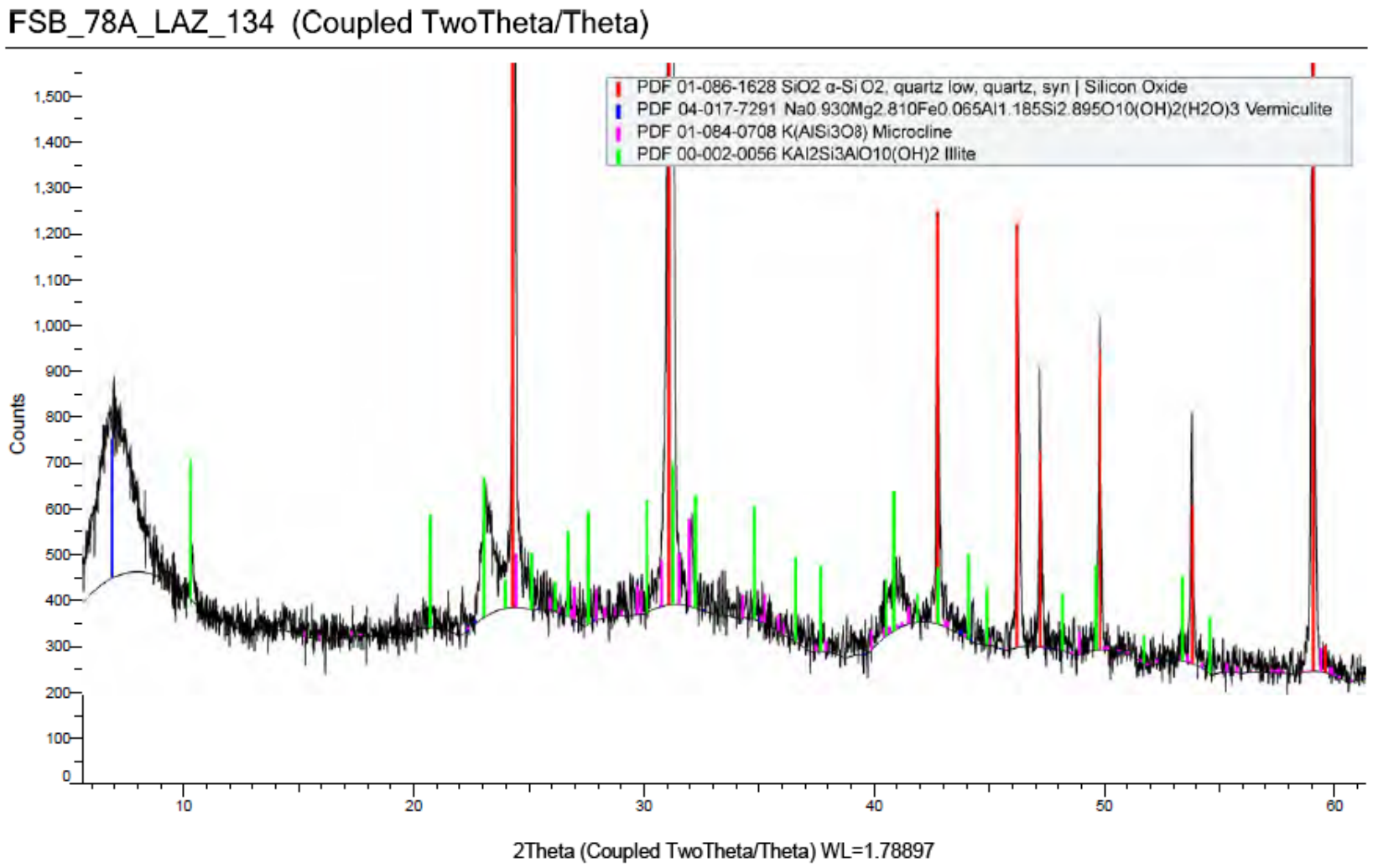

Figure 6-29. Zoomed bulk XRD diffraction pattern: FSB-78A, LAZ, 134 ft

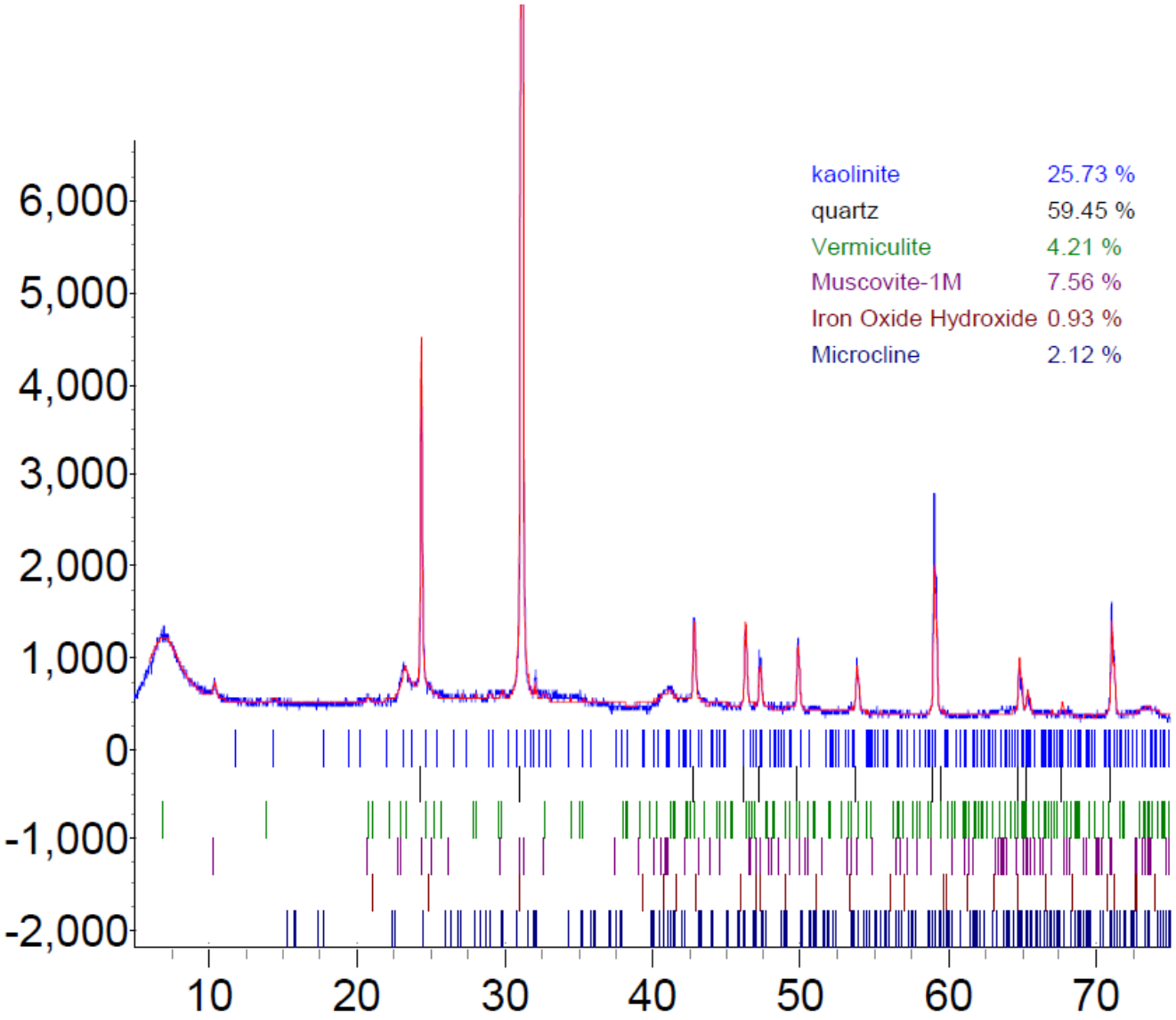

Figure 6-30. Bulk XRD identification and semi-quantification: FSB-78A, LAZ, 134 ft

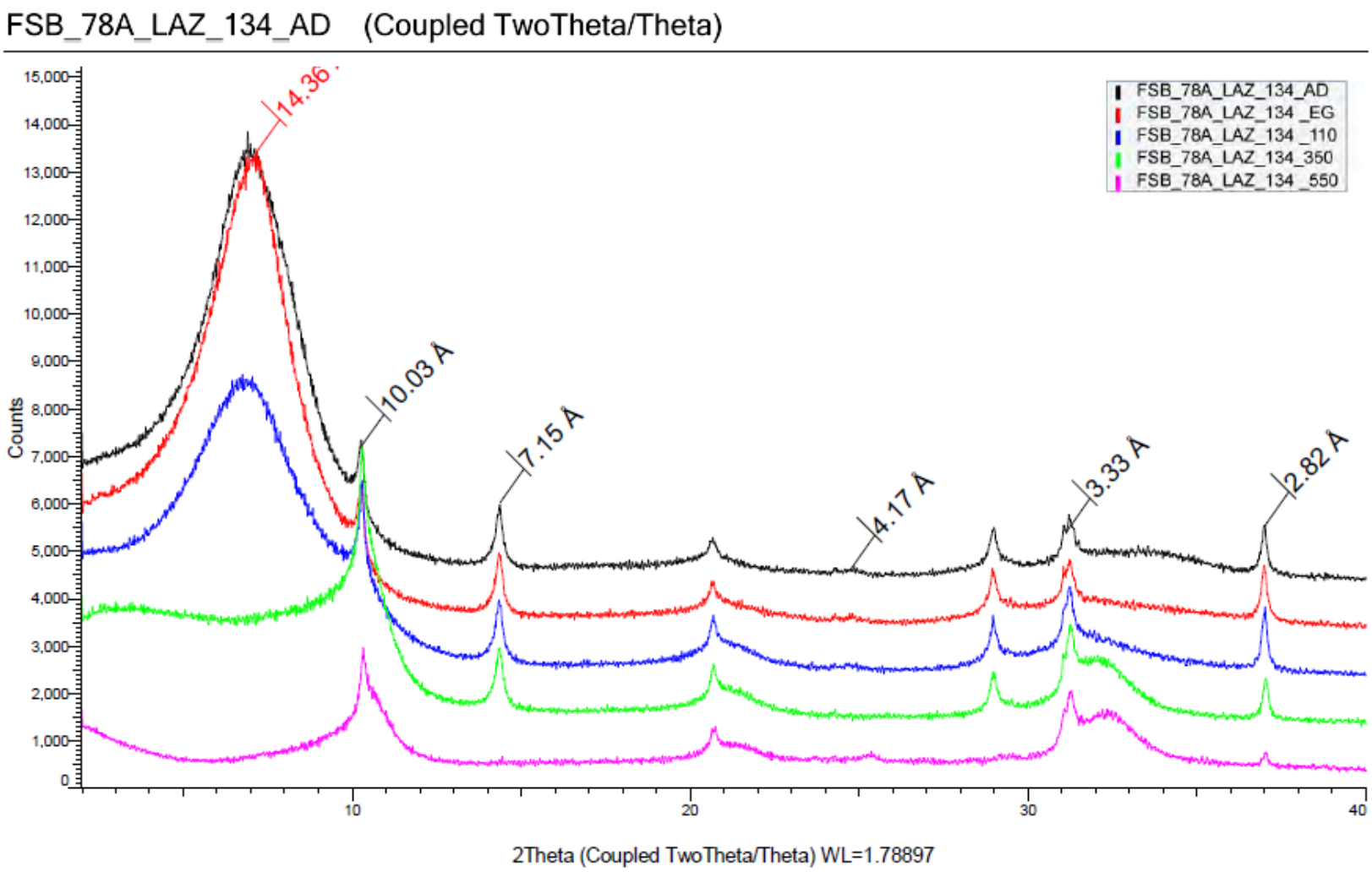

Figure 6-31. Clay fraction XRD diffraction pattern: FSB-78A, LAZ, 134 ft

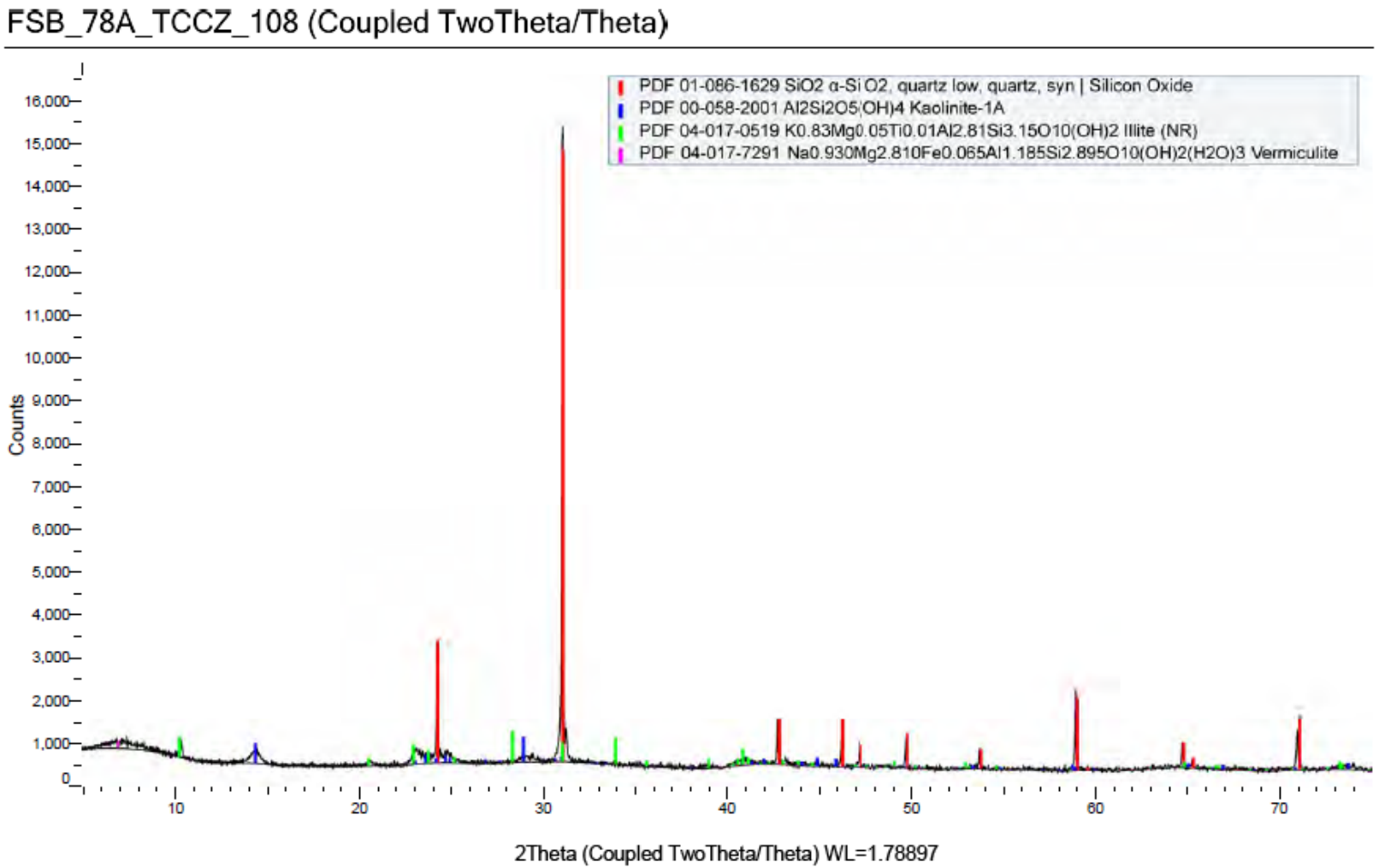

Figure 6-32. Bulk XRD diffraction pattern: FSB-78A, TCCZ, 108 ft

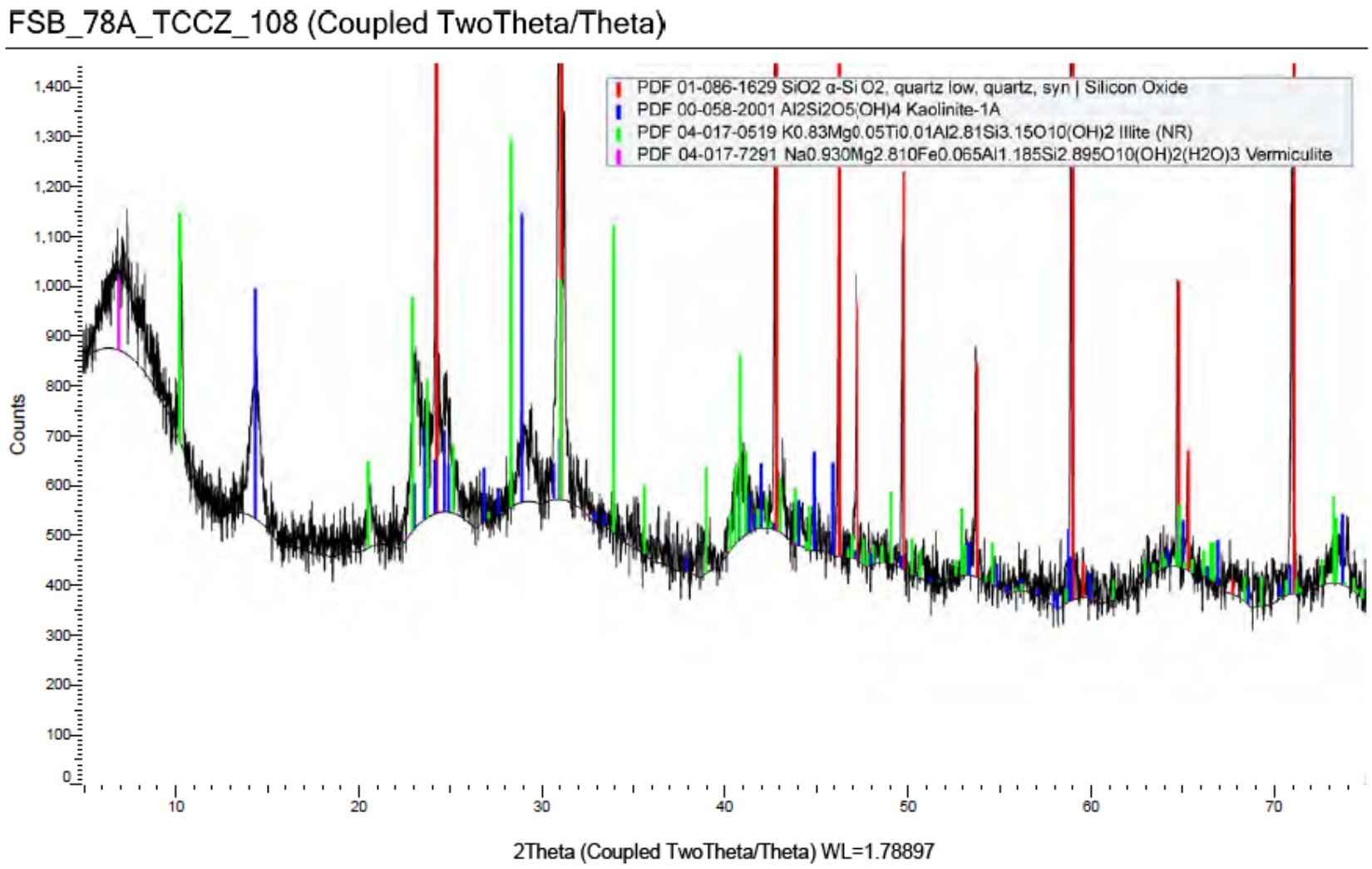

Figure 6-33. Zoomed bulk XRD diffraction pattern: FSB-78A, TCCZ, 108 ft

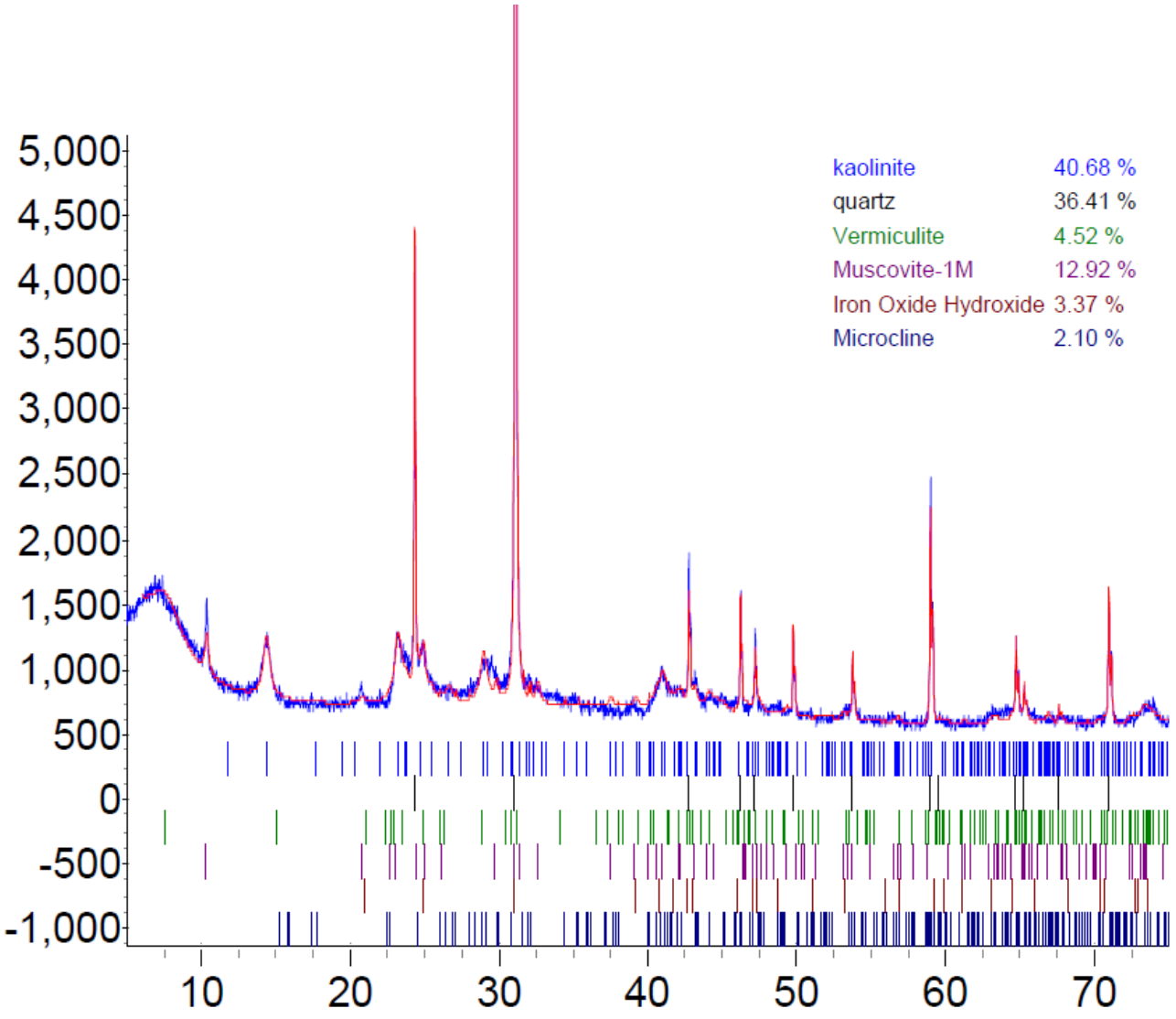

Figure 6-34. Bulk XRD identification and semi-quantification: FSB-78A, TCCZ, 108 ft

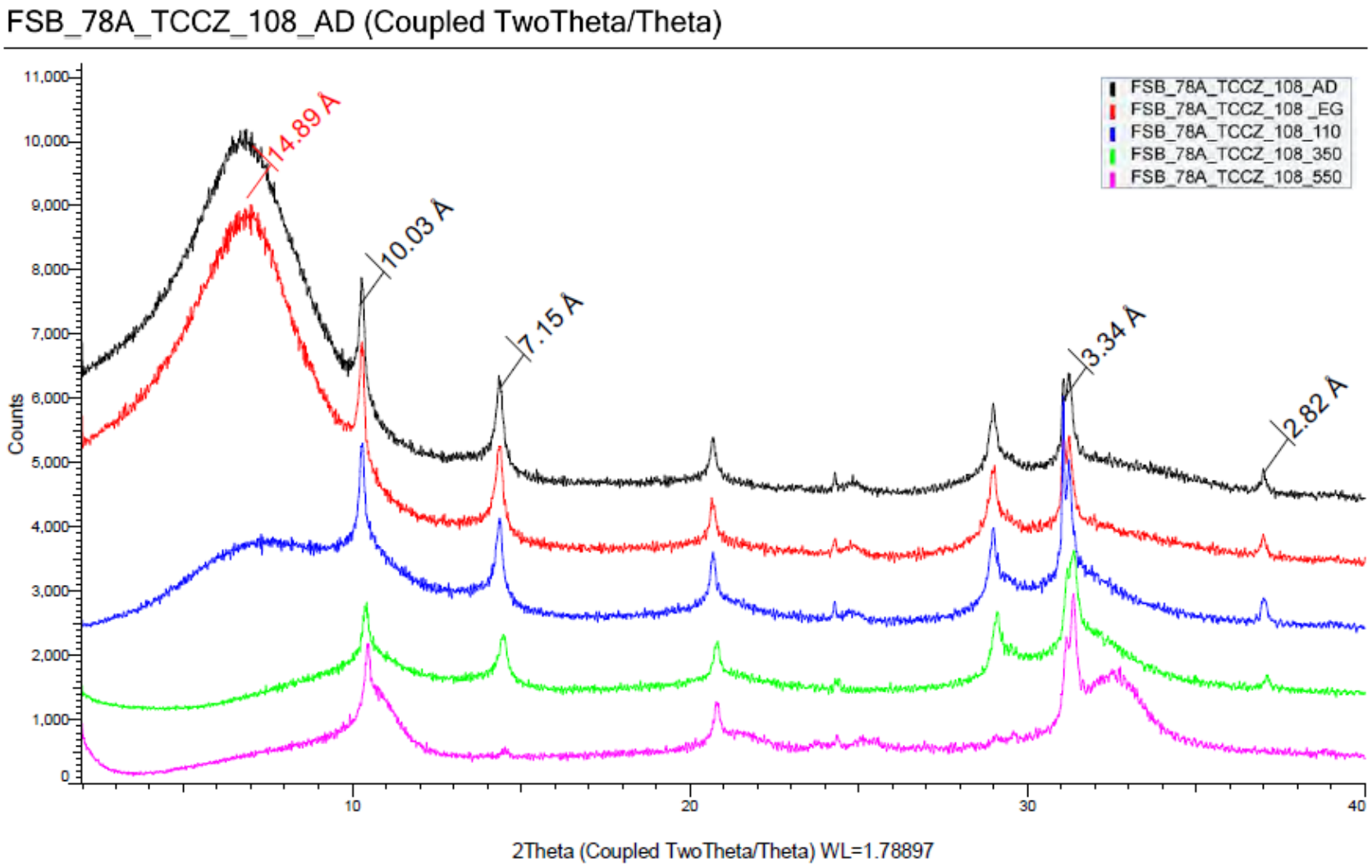

Figure 6-35. Clay fraction XRD diffraction pattern: FSB-78A, TCCZ, 108 ft

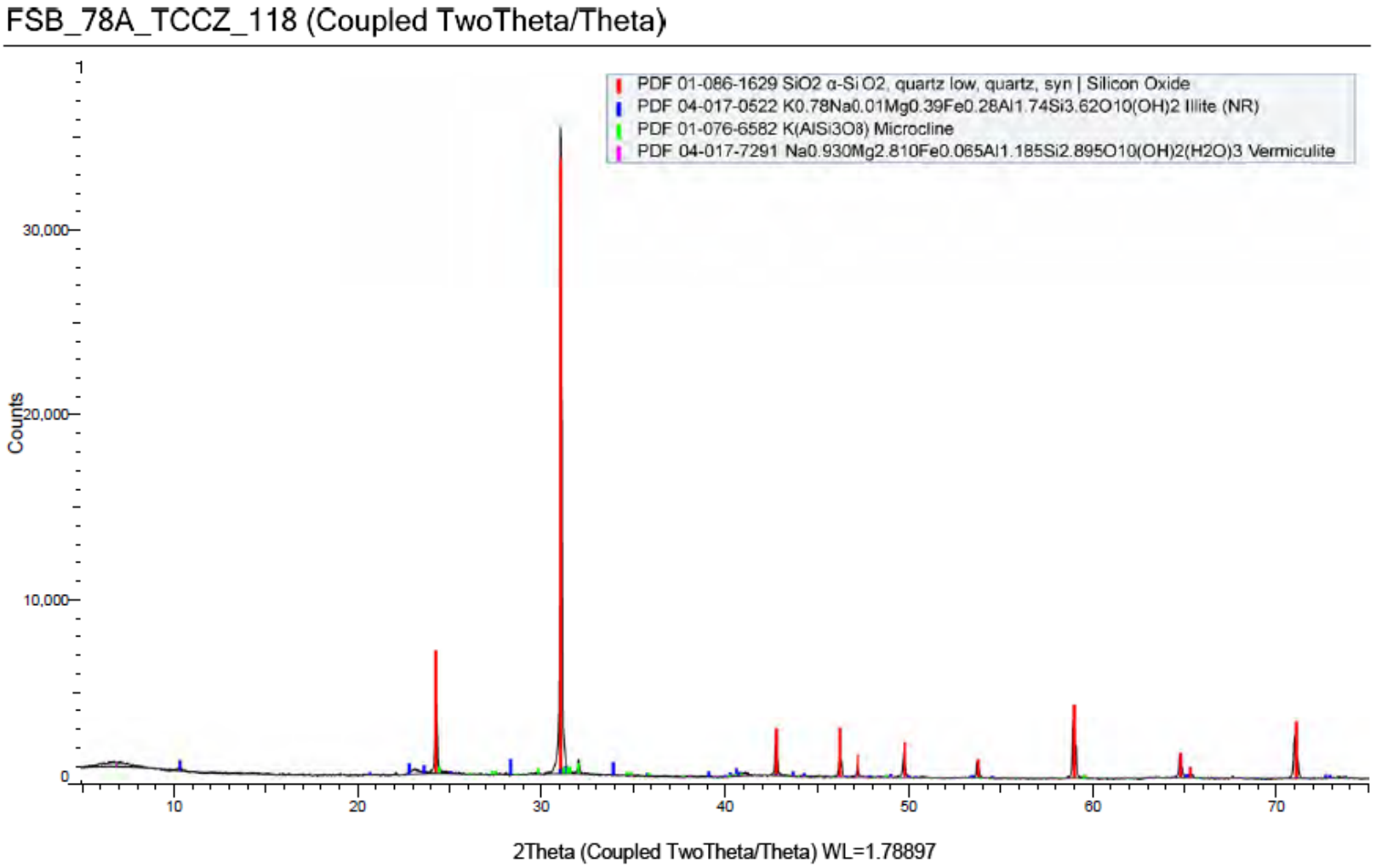

Figure 6-36. Bulk XRD diffraction pattern: FSB-78A, TCCZ, 118 ft

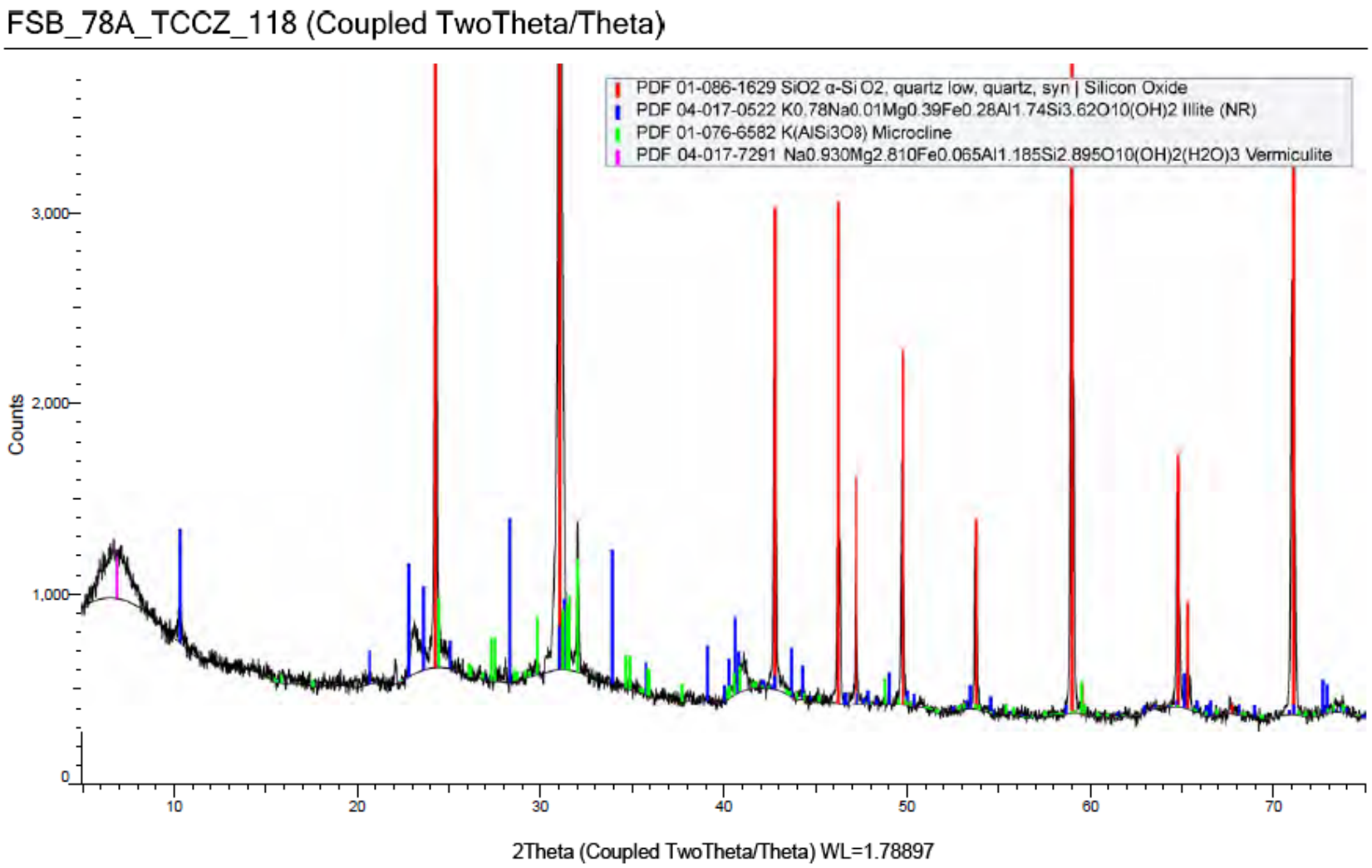

Figure 6-37. Zoomed bulk XRD diffraction pattern: FSB-78A, TCCZ, 118 ft

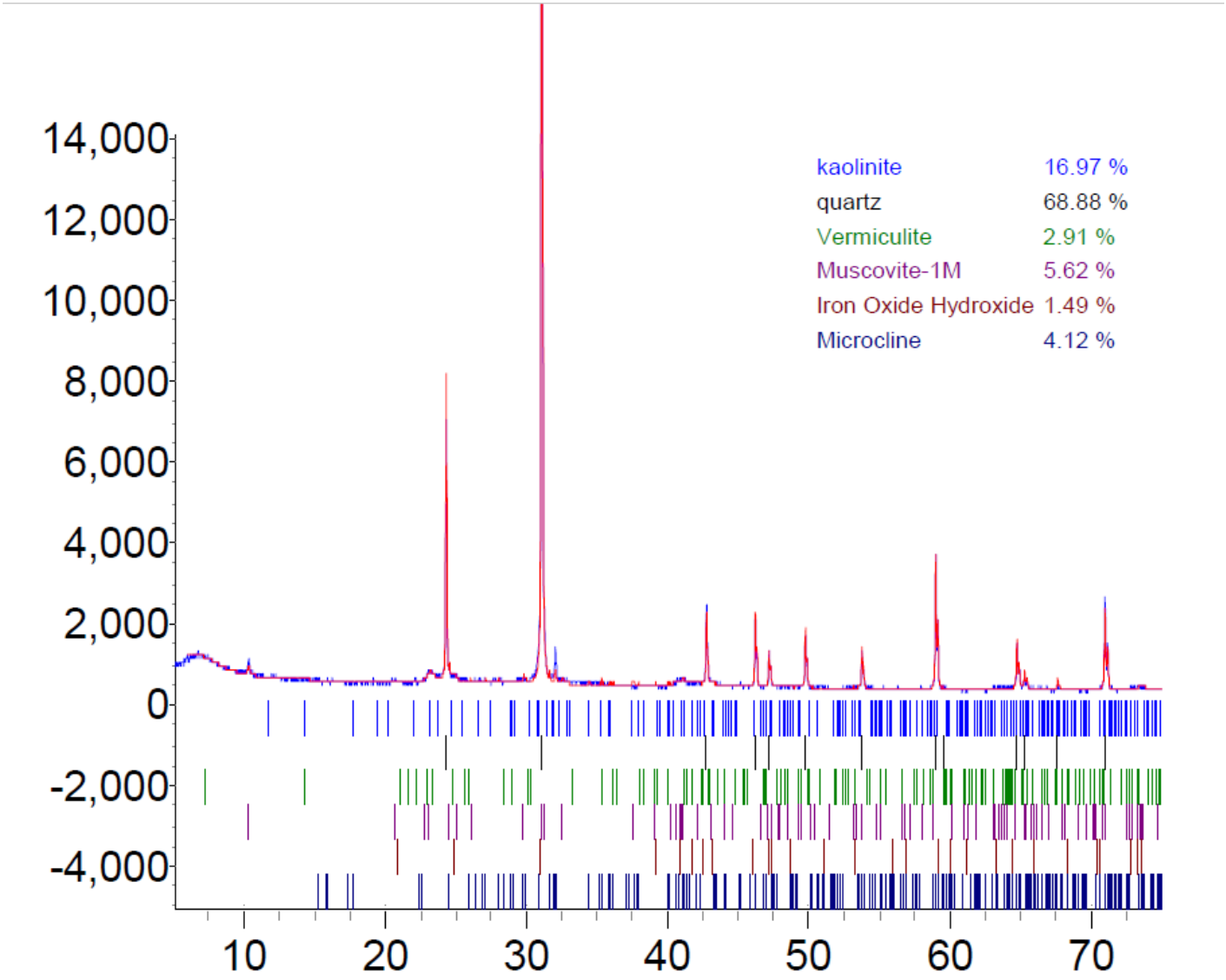

Figure 6-38. Bulk XRD identification and semi-quantification: FSB-78A, TCCZ, 118 ft

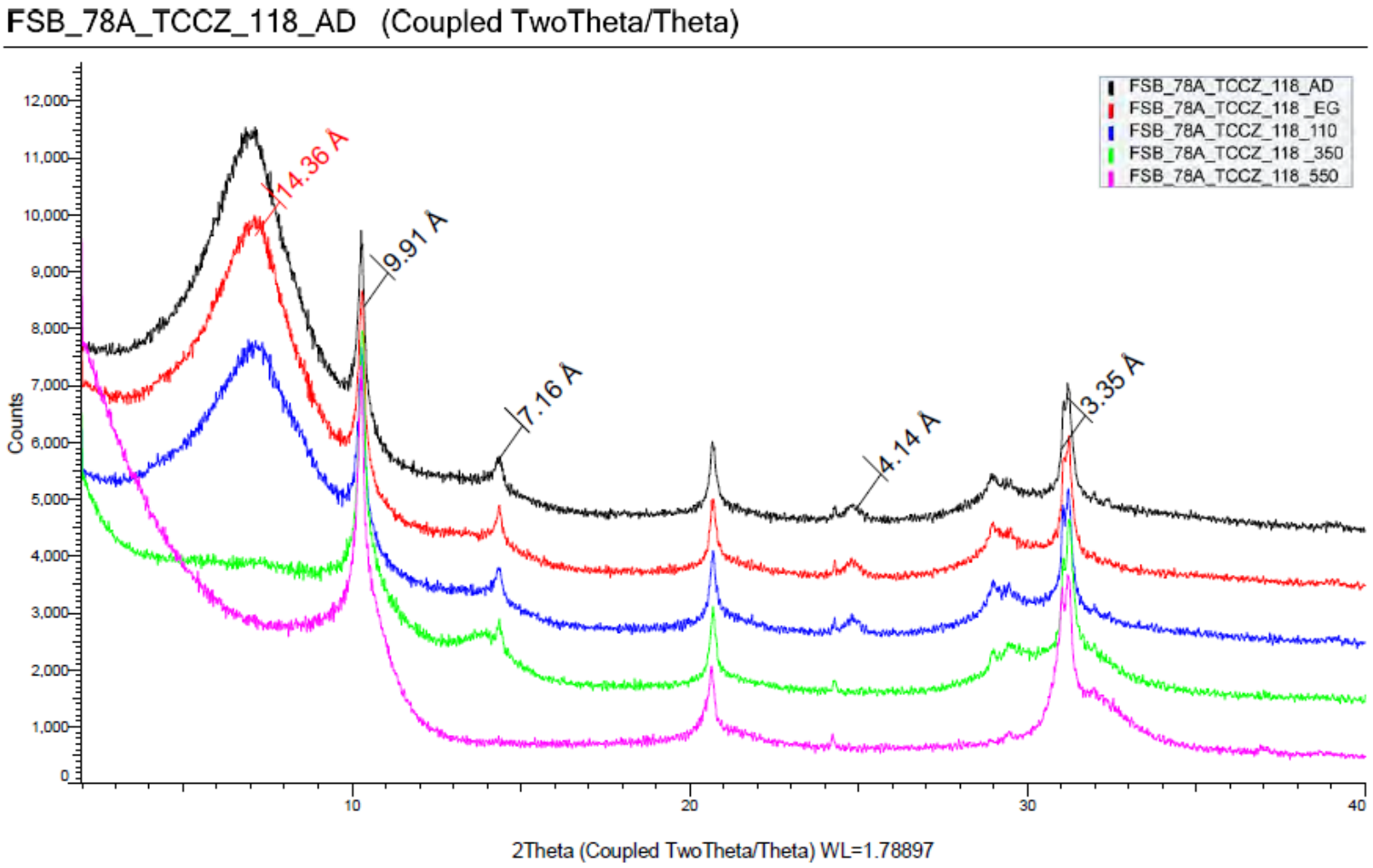

Figure 6-39. Clay fraction XRD diffraction pattern: FSB-78A, TCCZ, 118 ft

Distribution:

Kathryn.Taylor-Pashow@srnl.doe.gov	william.ramsey@srnl.doe.gov
cj.bannochie@srnl.doe.gov	boyd.wiedenman@srnl.doe.gov
marion.cofer@srnl.doe.gov	sue.clark@srnl.doe.gov
william.bates@srnl.doe.gov	sharon.marra@srnl.doe.gov
alex.cozzi@srnl.doe.gov	vahid.majidi@srnl.doe.gov
connie.herman@srnl.doe.gov	sarah.hodges@srnl.doe.gov
brady.lee@srnl.doe.gov	Kalyn.Loudermilk@srnl.doe.gov
joseph.manna@srnl.doe.gov	Heather.Capogreco@srnl.doe.gov
gregg.morgan@srnl.doe.gov	tony.polk@srs.gov
brandi.clark@srnl.doe.gov	nixon.peralta@srs.gov
frank.pennebaker@srnl.doe.gov	ombreyan.Broadwater@srs.gov
eric.skidmore@srnl.doe.gov	billy.hudson@srs.gov
mary.whitehead@srnl.doe.gov	jeffrey.crenshaw@srs.gov
clint.gregory@srnl.doe.gov	joseph.smith@srs.gov
c.diprete@srnl.doe.gov	angelia.holmes@srs.gov
morgana.whiteside@srnl.doe.gov	karen.morrow@srs.gov
holly.hall@srnl.doe.gov	william.ostrum@hq.doe.gov
donna.byrdy@srnl.doe.gov	aaron.white@em.doe.gov
jennifer.wohlwend@srnl.doe.gov	Kristen.Ellis@em.doe.gov
corey.radtke@srnl.doe.gov	rodrigo.rimando@em.doe.gov
jason.lashley@srnl.doe.gov	todd.shrader@em.doe.gov
carol.eddy-dilek@srnl.doe.gov	ming.zhu@em.doe.gov
brian02.looney@srnl.doe.gov	grover.chamberlain@em.doe.gov
john.mayer@srnl.doe.gov	nicholas.machara@em.doe.gov
tyler.chavous@srnl.doe.gov	john.lee@em.doe.gov
david.diprete@srnl.doe.gov	melanie.pearson@em.doe.gov
simona.murph@srnl.doe.gov	jean.pabon@em.doe.gov
michael.stone@srnl.doe.govchristine.langton@srnl.doe.gov	Hansell.Gonzalez-Raymat@srnl.doe.gov
daniel.mccabe@srnl.doe.gov	Emily.Fabricatore@srnl.doe.gov
utpal.roy@srnl.doe.gov	mdenham@panoramic.consulting
	Records Administration (EDWS)